Cell swelling enhances GPCR ternary complex formation, underpinning the potentiation of β2 adrenergic receptor-mediated cAMP response

Alexei Sirbu[1], Marc Bathe-Peters [1], Asuka Inoue[2], Martin J. Lohse[1,3,4], Paolo Annibale[1,5]*

[1] Max Delbrück Center for Molecular Medicine in the Helmholtz Association (MDC), 13125 Berlin, Germany

[2] Tohoku University, 980-8578 Japan

[3] ISAR Bioscience Institute, 82152 Munich-Planegg, Germany

[4] Leipzig University, Medical Faculty, Rudolf-Boehm-Institute of Pharmacology and Toxicology, 04107 Leipzig, Germany

[5] School of Physics and Astronomy, University of St Andrews, KY169SS St Andrews, United Kingdom

*pa53@st-andrews.ac.uk

Abstract

G protein-coupled receptors' conformational landscape can be affected by their local, microscopic interactions within the cell plasma membrane. We employ here a pleiotropic stimulus, namely osmotic swelling, to alter the cortical environment within intact cells and monitor the response in terms of receptor function and downstream signaling. We observe that in osmotically swollen cells the β2-adrenergic receptor, a prototypical GPCR, favors an active conformation, resulting in cAMP transient responses to adrenergic stimulation that have increased amplitude. The results are validated in primary cell types such as adult cardiomyocytes, a model system where swelling occurs upon ischemia-reperfusion injury. Our results suggest that receptors' function is finely modulated by their biophysical context, and specifically that osmotic swelling acts as a potentiator of downstream signaling, not only for the β2-adrenergic receptor, but also for other receptors, hinting at a more general regulatory mechanism.

Introduction

One of the tenets in G protein-coupled receptors (GPCR) pharmacology is the ternary complex model, stating that a high affinity state characterized by increased receptor-G protein coupling also correlates to increased affinity of the receptor towards its agonist, since the intracellular G protein coupling stabilizes the active receptor conformation[1]. Further to the development of this model, our understanding of GPCRs' function has evolved from two-state switches to rheostats exploring a complex conformational landscape, that in turn entails a broad repertoire of intracellular interactions[2]. Prototypical examples are molecules from the extracellular space acting as allosteric modulators of receptor function: they favor specific conformations -further stabilized upon ligand binding- that are different from those that would be observed in the absence of the modulator[3].

An emerging concept is that changes of the biophysical context around the receptor can 'allosterically' modulate its function. Mechanistically this involves the action of accessory proteins[4], local lipid composition[5], interaction with intracellular scaffolds[6], and -as highlighted recently- local curvature[7]. These interactions can modulate each of the canonical signaling steps (ligand binding, ternary complex formation with cognate G protein, β-arrestin recruitment, trafficking), endowing these receptors with a broad modulatory repertoire able to nuance specific signals in a dynamic and flexible way in space and time.

Some of the interactions may be local, receptor-specific and associated with specific modulatory proteins, such as Receptor Associated Modifying Proteins (RAMPs)[4]. Other interactions may be more spatially diffuse, such as the interaction of GPCRs containing a PDZ binding sequence with the cortical actin, or, as it was proposed more recently, the segregation of selected GPCRs to areas of higher or shallower curvature within the cell membrane[8]. Along these lines, we observed recently µm-sized receptor-specific segregation to a subcellular compartment, such as the T-tubular network of adult cardiomyocytes, characterized by high local curvature[9].

While the hypothesis that subcellular receptors' localization and local biophysical interactions may indeed modulate -to a sizable extent- their behavior is being increasingly explored[10,11], nonetheless the

actual molecular mechanisms underpinning such effects are harder to unravel. These may be ascribed to heterogeneities in lipid composition of the plasma membrane[12], such as caveolae, or in the local density of the cortical actin network and the variability of its interactions with the membrane[13]. Moreover, if modulation of GPCR signaling indeed occurs across multiple length-scales at the plasma membrane, from nanometer to micrometer scale, its microscopic identification challenges current technologies[14].

At the receptor level, this modulation ultimately relies on the notion that GPCRs are mechanosensitive molecules, i.e. able to register local stresses and forces acting on their transmembrane domains as well as intra- and extracellular loops, resulting in conformational landscapes favoring specific downstream signaling outcomes[15]. Indeed, the effect of mechanical tension along the plasma membrane has been invoked as the cause for the ligand-independent activation of selected GPCRs, such as the bradykinin B2 receptor[16], the angiotensin II type 1 receptor[17] or the Histamine H1 receptor[18].The latter work identified helix 8 as the essential structural motif for GPCR mechanosensitivity, beyond the more established force sensing mechanisms of adhesion GPCRs, that instead rely on autocatalytic cleavage of the N-terminal domain.

We reasoned that osmotic swelling, a process that occurs in several (patho-)physiological settings may offer the type of pleiotropic biophysical modulation that we are seeking to test such hypothesis. Cell swelling is associated to a complex rearrangement of the cell membrane environment, ranging from alteration of local geometry, F-actin remodulation and increases in cell surface originating from flattening of the membrane, not unlike ironing out wrinkles in a cloth[19,20]. We decided to focus on β-adrenergic receptors (β-ARs), both because of their prototypical nature (i.e. they couple to the stimulatory G protein and elicit an increase in cAMP upon $G\alpha_s$ interaction with the adenylyl cyclase (AC)) but also because they display a rich conformational landscape[21] and the role of cortical actin in connection to their localization and signaling, in particular the β2-AR, is well documented[6,22].

Our key observation is that swollen cells yield sizably higher cAMP concentrations in response to β-ARs stimulation than non-swollen cells. To pinpoint at what step this occurs, we set out to explore the whole signaling cascade of the β2-AR. Each step of the cascade was investigated with a specific fluorescent spectroscopy method, ranging from TIRF to fluorescence polarization and FRET biosensing, that allowed us working in intact cells. We could determine that this effect does not arise from alterations at the level of AC catalytic rates, nor by alterations of receptors trafficking, but rather by a distinctive increase in receptor-G protein coupling, mirrored by an increased affinity of the agonist isoproterenol for the receptor.

These findings demonstrate a novel way of modulating GPCR conformation by biophysical factors, while also showing a previously unappreciated effect of cell swelling on 2nd messenger production, which has the potential to be transferred to other GPCRs or transmembrane receptors acting in a broad range of physiological settings.

Results

To gauge the effect of osmotic swelling on the downstream signalling cascade of the β-ARs we first employed FRET-based cAMP fluorescence biosensors. The layout of our readout is schematically depicted in **Figure 1a**. When measuring FRET in a single cell under a microscope, it is possible to display the degree of energy transfer between the donor and acceptor of the sensor in a false-color scale, that will change upon agonist addition (100 pM isoproterenol (Iso) in our case). The relative change between the swollen and control state of a representative HEK293 cell is displayed in **Figure 1b**, next to the donor and acceptor channels separately. Upon addition of the swelling medium (containing the same concentration of Iso as the isotonic medium) to a cell expressing endogenous levels of receptors, the cAMP response is sizably increased. We then moved to a high-throughput configuration where the signal from tens of thousands of cells was observed in 96-well plates using a fluorescent plate reader. A representative trajectory of intracellular cAMP concentration (proportional to the change in normalized FRET ratio) upon Iso addition in control vs swollen cells is displayed in **Figure 1c**. Trajectories from swollen cells are displayed in blue throughout the manuscript, as opposed to cells maintained in isotonic medium (control) which are displayed in red. A strong peak in cAMP concentration is observed in the swollen cells a few minutes upon non-saturating Iso addition. Saturating cAMP levels are then obtained upon Fsk/IBMX stimulation for normalization purposes. We

shall note that the results observed are independent of normalization to Fsk/IBMX (**Supplementary Figure 1a),** that the raw data display clear antiparallel traces for donor and acceptor, both in control as well as in swelling conditions (**Supplementary Figure 1b**) and that the response to FSK/IBMX is not sensitive to osmotic swelling (**Supplementary Figure 1c**). When repeated for increasing concentrations of the agonist, ranging from 1 pM up to 100 nM concentration, it was thus possible to build a concentration response curve, as displayed in **Figure 1d**. We observe a statistically significant difference in the log(EC_{50}), which drops from -9.28 ± 0.12 to -9.8 ± 0.1 for the average curves. The peak cAMP response in swollen cells then declines within a few minutes to a steady state comparable to the concentration observed in the controls (**Supplementary Figure 1d**). To rule out any effect of osmotic swelling on the readout of our fluorescence biosensor, a concentration response curve was calculated in the two conditions using the cell permeable cAMP derivative 8-Br-cAMP, displaying overlapping curves for swollen and control cells (**Supplementary Figure 1e**). Individual log(EC_{50}) values from separate experiments are displayed for the two conditions in **Figure 1e**, which in turn allows to appreciate the fact that the observed difference applies only to the transient cAMP response and not to the steady state concentration. We verified that our time-resolved results using FRET biosensors are matched by an endpoint assay (10 minutes after stimulation), such as the AlphaScreen that is based on the readout of energy transfer between donor and acceptor beads, connected by biotinylated cAMP which is then displaced by the cAMP from cell lysates **(Supplementary Figure 1f)**.

Interestingly, similar results can be obtained when looking at cells stimulated with partial β-adrenergic agonists, such as salbutamol, salmeterol and terbutaline (**Supplementary Figure 2a-c**). The specificity of the effects for both β1-AR and β2-AR was tested by overexpressing them separately in a cellular background devoid of endogenous β-AR expression, such as Chinese Hamster Ovary cells (CHO), as displayed in **Supplementary Figure 2d-e**. When challenging other G_s coupled receptors endogenously found in HEK293 cells, such as the histamine H_2 receptor or the melanocortin receptors **(Supplementary Figure 2 f-g)** a similar outcome in terms of cAMP response can be observed upon osmotic swelling. Moreover, we observed a similar behavior at the level of Gi protein activation[23] for the μ opioid receptor (μOR) upon stimulation with the synthetic agonist DAMGO (**Supplementary Figure 3a-c)**.

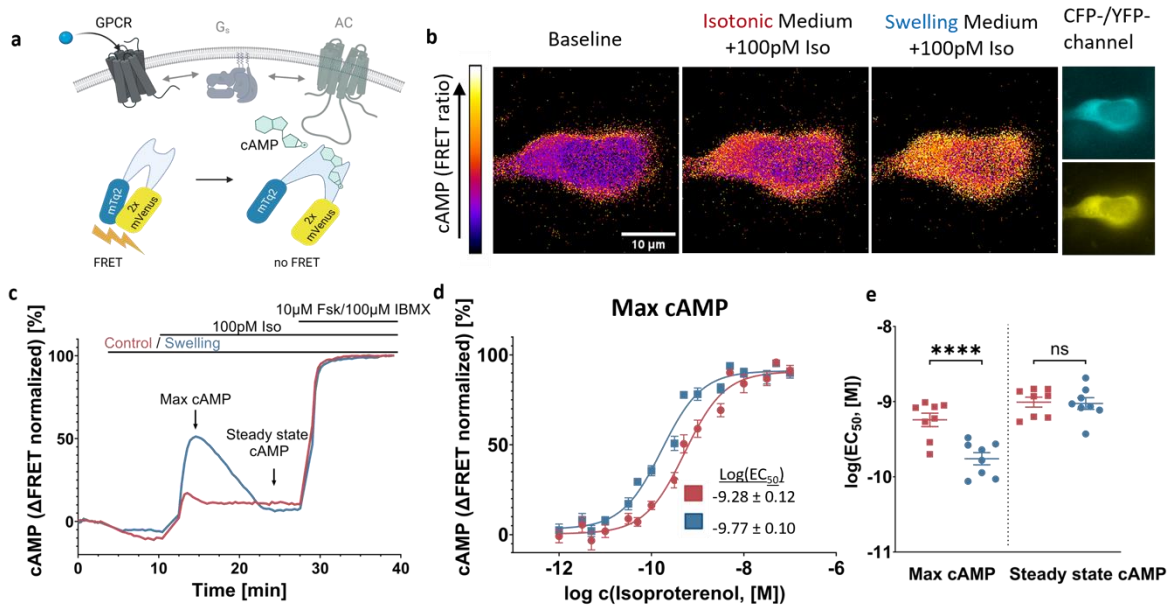

Figure 1 Cell swelling increases β-adrenergic-mediated cAMP production in HEK293 cells.

a Schematics of GPCR-mediated cAMP production and its detection by a FRET biosensor; **b** Representative images of a HEK293 cell stably expressing cytosolic Epac-S^{H187} [24] showing acceptor/donor ratio in false colour; the cells are exposed to 100 pM isoproterenol first in isotonic (300 mOsm) and subsequently in swelling medium (200 mOsm); **c** representative curve showing kinetics of acceptor/donor ratio measured in HEK293 cells stably expressing Epac-S^{H187} in a microplate reader (normalized to baseline and 10 µM forskolin + 100 µM IBMX); **d** averaged concentration response

curves representing maximal cAMP concentrations, as indicated in (**c**) (mean ± SEM; n = 8 plates form 7 independent experiments); **e** log(EC_{50}) values from individual experiments comparing swelling and control condition for maximal and steady state cAMP concentrations (statistical analysis performed by a paired two-tailed t-test).

We then addressed the question if this remarkable behavior was observed also in primary cells that are known to be subject to osmotic swelling in physiological or pathophysiological conditions, namely adult ventricular cardiomyocytes (CM): CMs undergo swelling during the reperfusion phase following ischemic shock[25]. Murine adult ventricular CMs were isolated and seeded on multiwell imaging plates and imaged on the same day, after labeling using a cell membrane dye (**Materials and Methods)**. Upon exposure to the swelling media the CMs display a visible increase in volume, as illustrated in **Figure 2a**. The increase was quantified as the relative change in cell area, as detected in 2D confocal sections (**Figure 2b, Supplementary Figure 4a-b).** The volume of the cells appears to increase for approximately 10-15 minutes, before saturating. This is in line with what is observed for HEK293 cells, where saturation is reached after approximately 15 minutes from the onset of osmotic swelling (**Supplementary Figure 4g-h)**. Following the same approach used to generate the data in **Figure 1b**, we employed CMs isolated from a transgenic mouse expressing the Epac1-camps cAMP sensor[10] and imaged them under a microscope (**Supplementary Movie 1**). The relative changes in cAMP concentration upon agonist addition were quantified for each cell, and representative traces for a control vs a swollen CMs are displayed in **Figure 2c**. Upon osmotic swelling, the cAMP response to non-saturating concentrations of Iso was clearly enhanced, consistent with the observations reported in **Figure 1** for HEK293 cells.

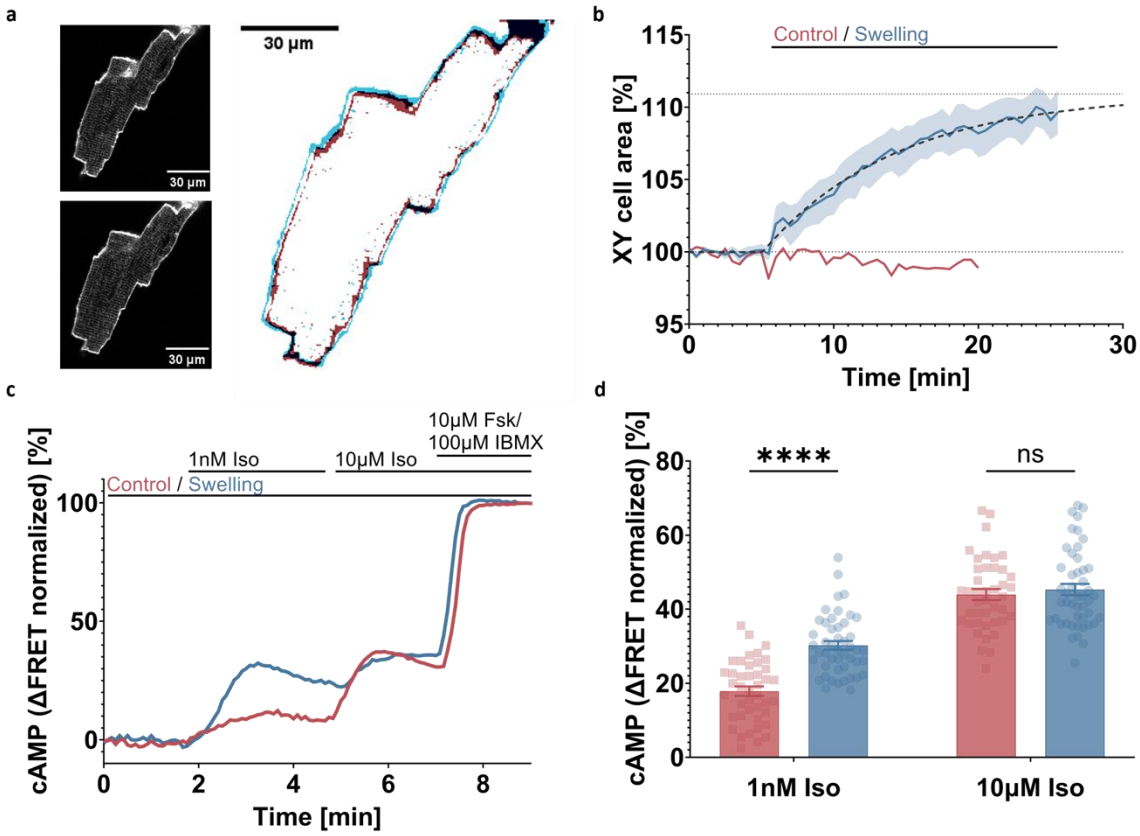

Figure 2 Cell swelling increases β-adrenergic mediated cAMP production in adult mouse ventricular cardiomyocytes (CM)

a Confocal images of CM under isotonic conditions (upper inset) and after 20 minutes of exposure to swelling medium (lower inset), with an overlay of cell edges under both conditions (main); **b** average curve showing the area of a confocal CM slice (mean ± SEM; n = 6 cells from 3 independent experiments); **c** representative curve showing kinetics of acceptor/donor ratio measured in CM stably

expressing Epac1-camps under an epifluorescence microscope (normalized to baseline and 10 µM forskolin + 100 µM IBMX); **d** maximal cAMP concentrations reached upon stimulation with 1 nM and 10 µM Iso respectively, normalized to 10 µM forskolin + 100 µM IBMX (mean ± SEM; n = 42 (control) and 47 (swelling) cells from 3 independent experiments; statistical analysis performed by an unpaired two-tailed t-test).

The data for 1 nM and 10 µM iso additions are summarised in **Figure 2d** and illustrate that cAMP signalling is enhanced in swollen adult CMs for Iso stimulations around the sub-maximal concentration[17], while being equal at saturating concentration. Albeit it was not possible to generate a full concentration response curve based on single cell images, this data reports an effect clearly consistent with the one displayed in **Figure 1d**. Overall, these results point to the potential (patho-)physiological relevance of this mechanism.

We thus set out to identify the molecular determinants of the observed changes in cAMP response in swollen cells. Since swelling is a pleiotropic modulator of cell homeostasis, we systematically investigated all steps of the signalling cascade, from PDE-mediated degradation of cAMP up to G protein coupling. We graphically summarised these steps in **Figure 3a** (1-6), that acts as a legend to the other panels of **Figure 3**. In **Figure 1** we have reported on (1), namely the observed increase in cytosolic cAMP. As our next step we measured cAMP concentrations with a biosensor localized to the plasma membrane (Epac1-camps-CAAX)[23] to test if the observed cytosolic increase in cAMP can be ascribed to changes in local membrane pools (2). This explanation could be excluded after observing an analogous pattern in local cAMP concentrations at the cell membrane (**Supplementary Figure 5a)**. We then set to rule out that altered receptor trafficking (3), namely decreased desensitization or downregulation supported by clathrin-mediated endocytosis could be the origin of the observed effect[26]. First, we monitored whether baseline receptor expression was altered at the plasma membrane of swollen vs control cells, observing that the average number of heterologously expressed β2-AR is not affected by the treatment (**Supplementary Figure 5h-i**) We then treated cells with Dyngo-4a, a well characterised dynamin inhibitor. **Supplementary Figure 5b** illustrates that the cAMP production increase reported in **Figure 1** is still present in HEK293 cells treated with 10 µM Dyngo-4a. Moreover, the decrease in the number of receptors at the plasma membrane in cells where internalization takes places is comparable between control and swollen cells after 10 minutes of Iso stimulation, confirming that swelling has limited to no effect on receptor trafficking in the observed timeframe (**Supplementary Figure 5j**). We then investigated the potential role of altered phosphodiesterase activity[27] (4), as altered degradation rates (in this case reduced) may account for the observed increase in cAMP concentration transients in swollen cells.

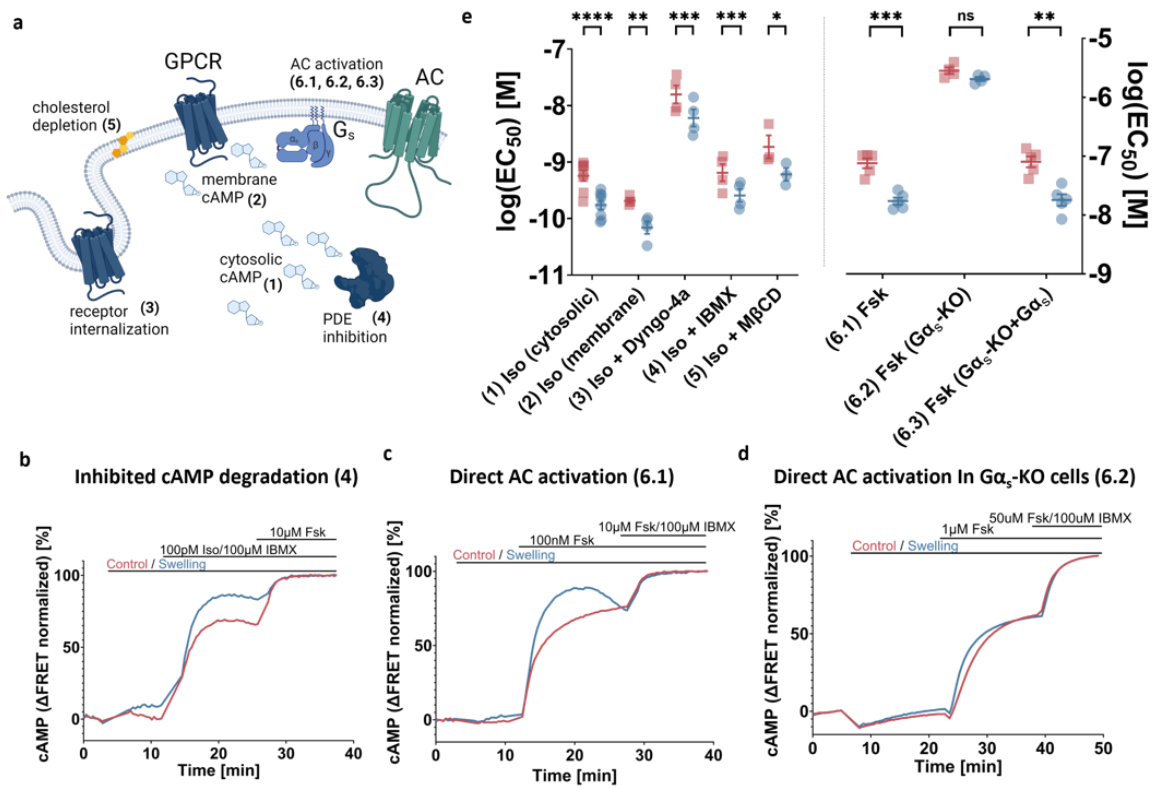

Figure 3 Impact of cell swelling on the molecular steps of the β-adrenergic signalling cascade

a Schematics of key steps of the signaling cascade that may be affected by swelling and were assessed under following conditions: (1) cytosolic cAMP upon Iso stimulation, (2) local cAMP at the plasma membrane upon Iso stimulation measured with an Epac1-Camps-CAAX sensor, (3) cytosolic cAMP measured upon Iso stimulation after treatment with 10μM Dyngo-4a for 30 min, (4) cytosolic cAMP measured upon Iso stimulation with simultaneous addition of 100μM IBMX, (5) cytosolic cAMP measured upon Iso stimulation under cholesterol depletion after incubation for 30 minutes with 10mM methyl-β-cyclodextrine, (6) cytosolic cAMP measured upon Fsk stimulation in wt Gαs phenotype (6.1), Gαs-KO cells (6.2) and Gαs-KO cells transiently transfected with Gαs (6.3); **b-d** representative kinetic cAMP concentration curves obtained under respective conditions described in a; **e** log(EC50) values from individual experiments comparing swelling and control condition for maximal cAMP concentrations under conditions listed in (a) (mean ± SEM, n = at least 3 independent experiments; statistical analysis performed by paired two-tailed t-tests);

The addition of the pan-PDE inhibitor IBMX, at the concentration of 100 μM, did not abolish the observed relative increase in transient cAMP concentration in the swollen cells, as illustrated in **Figure 3b** and **Supplementary Figure 5c[27].** Cholesterol sequestration (5) using methyl-β-cyclodextrin (MβCD) did not abolish the observed effect either (**Supplementary Figure 5d)**. We thus moved upstream along the signalling cascade: the next target is the family of enzymes responsible for cAMP synthesis, namely ACs (6). ACs are canonically activated by the GTP-bound $G\alpha_s$ subunit of the heterotrimeric G protein. The diterpene forskolin and $G\alpha_s$ have a synergistic/cooperative action in activating ACs[28-30]. In cells possessing endogenous $G\alpha_s$, direct stimulation of AC by forskolin leads to marked cAMP concentration increases, and the differential effect elicited by cell osmotic swelling persists (**Figure 3c and Supplementary Figure 5e**). However, interestingly, in cell lines carrying a $G\alpha_s$ knockout[31], we observed that any effect of osmotic swelling upon the amplitude of the cAMP concentration increase (**Figure 3d and Supplementary Figure 5f**) is lost. The effect is however recovered upon heterologous transfection of $G\alpha_s$ in the knockout lines (**Supplementary Figure 5g**), thus pinning on the α subunit of the heterotrimeric G_s protein a key role in modulating the signalling cascade's response to osmotic swelling.

The overall results are summarised as log(EC_{50}) values in **Figure 3e**, that shows a consistent left-shift of the EC_{50} values of approximately half a log unit.

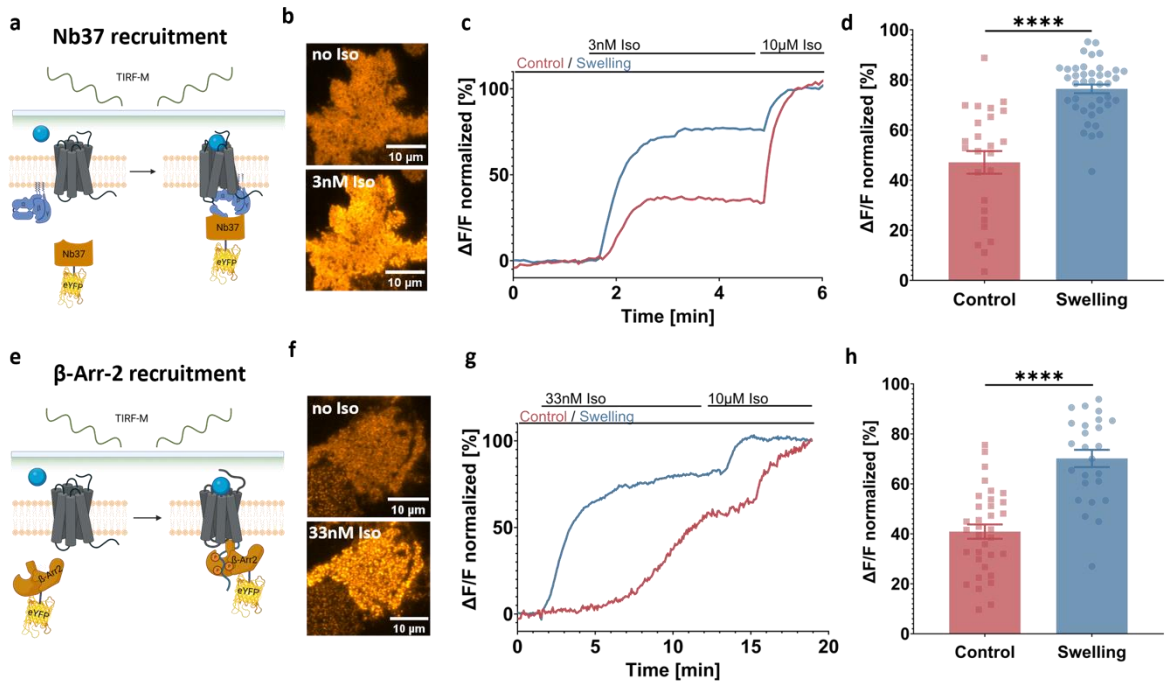

Figure 4 Swelling leads to an increased effector recruitment

a G_s activation by the β2-AR is monitored by recruitment of the fluorescently tagged nanobody 37 (Nb37) at the plasma membrane of the cell together with overexpression of heterotrimeric G_s; **b** representative TIRF-M images of Nb37-eYFP expressed in HEK293-AD cells before and after application of 3 nM isoproterenol; **c** representative curve showing relative increase of membrane fluorescence collected as first 3 nM, and then at saturating 10 µM concentration of isoproterenol is added to the cell (normalized to baseline and 10 µM Iso response); **d** relative fluorescence increase measured upon Nb37-eYFP recruitment upon 3 nM isoproterenol stimulation in swollen vs non-swollen cells (mean ± SEM; n = 25 (control) and 41 (swelling) cells from 3 independent experiments; statistical analysis performed by an unpaired two-tailed t-test); **e** recruitment of fluorescently tagged β-Arrestin-2 (β-Arr-2) by the β2-AR is monitored by its recruitment to the plasma membrane of the cell; **f** representative TIRF-M images of βArr-2-eYFP expressed in HEK293-AD cells before and after application of 33 nM isoproterenol; **g** representative curve showing relative increase of membrane fluorescence collected as first 33 nM, and then at saturating 10 µM concentration of isoproterenol is added to the cell (normalized to baseline and 10 µM Iso response); **h** relative fluorescence increase measured upon β-Arr-2-eYFP recruitment upon 33 nM isoproterenol stimulation in swollen vs non-swollen cells (mean ± SEM; n = 34 (control) and 25 (swelling) cells from 3 independent experiments; statistical analysis performed by an unpaired two-tailed t-test).

Based on these observations we decided to investigate further the role of G_s in mediating this remarkable response of cAMP transients to isoproterenol stimulation upon cell swelling. To do so we first asked the question if G_s activation by the receptor is enhanced in swollen cells. This question was addressed exploiting fluorescently tagged Nb37[32], reported to bind the active guanine-nucleotide-free $G\alpha_s$ found in the β2-AR - G_s ternary complex, as schematically illustrated in **Figure 4a**. After co-transfecting HEK293AD cells with β2-AR, the heterotrimeric G protein and Nb37-eYFP (as discussed in **Materials and Methods**) we imaged the cell basolateral membrane using Total Internal Reflection Fluorescence[33], to enhance the signal from membrane-associated Nb37-eYFP. This approach allowed us to monitor the membrane recruitment of Nb37-eYFP upon increasing concentrations of Iso (**Figure 4b, Supplementary movie 2**), and in turn confirm that in swollen cells the recruitment is enhanced at non-saturating isoproterenol concentrations (**Figure 4c**). Overall, the relative recruitment of Nb37 is

almost double in swollen cells than in the control (**Figure 4d**). This suggests that in swollen cells there is a sizably higher proportion of active G_s, hinting at a higher number of Iso - β2-AR - Gs ternary complexes, and therefore that osmotic swelling is a positive modulator of the receptor active conformation. These measurements are mirrored by measuring β-Arrestin-2 recruitment (**Figure 4e,f**), that is also enhanced in swollen cells (**Figure 4g**). We observed an almost twofold increase of eYFP-tagged β-arrestin-2 at the basal cell membrane upon non-saturating isoproterenol stimulation (**Figure 4h**). Interestingly, β-Arrestin-2 recruitment in swollen $G\alpha_s$ knockout cells was more prominent than in non-swollen cells (**Supplementary Figure 6**), suggesting that the effects observed at the arrestin are independent and not a downstream effect of $G\alpha_s$ activation.

If osmotic swelling indeed favors the formation of a ternary agonist-receptor-G_s (and/or agonist-receptor-β-arrestin-2) complex, we expect this to be reflected in a direct modulation of receptor conformation[34]. To test for this possibility, we conducted a set of assays aimed at monitoring agonist binding and receptor activation in intact cells. We employed a recently reported fluorescent ligand against the β-ARs, based on the inverse agonist carazolol[9], to conduct a set of fluorescence anisotropy binding assays[35], as graphically illustrated in **Figure 5a**. Simply put, as the the fluorescent ligand binds, its fluorescent anisotropy increases as a result of the reduction in rotational diffusion. As the fluorescence anisotropy increases proportionally to the fraction of bound ligand, it is possible to incubate cells overexpressing β2-AR as well as heterotrimeric G_s and Nb37 with a fixed concentration of fluorescent ligand, and then measure changes in fluorescence anisotropy as the fluorescent ligand is progressively displaced by increasing concentrations of the non-fluorescent Iso (**Figure 5b**). When comparing swollen and control cells, this leads to a shift in the ligand K_i, from $\log(K_i)=-6.77 \pm 0.03$ to -6.98 ± 0.04 (**Figure 5b**). Albeit the observed shift is small, it is significant, and it was consistently observed for each plate we investigated, as graphically summarised by the paired comparisons displayed in **Figure 5c.**

We can probe the formation a ternary agonist-receptor-transducer complex from the intracellular side by using a fluorescent probe acting as a proxy for the intracellular proteins recognising the active receptor conformation, namely fluorescently tagged Nb80 (Nb80-eYFP)[36], as schematically depicted in **Figure 5d**. By employing TIRF to measure nanobody recruitment, we can observe that there is a significant enhancement in Nb80 recruitment in swollen cells (**Figure 5e**), as also reflected by the full concentration response curve's ($\log(EC_{50})$) shifts from -7.96 ± 0.06 to -8.28 ± 0.09 (**Figure 5g**).

These results appear to be confirmed by conducting the experiments presented in **Figure 1** in cells preincubated with saturating (100µM) concentration of the β-AR antagonist propranolol. In these conditions, no cAMP elevation is observed in control cells upon either 1µM or 10µM, but the blockade appears to be abolished in swollen cells, where cAMP response can be observed already when 1µM isoproterenol is added to the cells (**Supplementary Figure 7a-b**). Interestingly, in swollen cells, a partial breakage of the propranolol blockade can be observed already at isoproterenol concentrations as low as 10 nM (**Supplementary Figure 7c-d)**. These observations support the notion that cell swelling transiently promotes an active receptor conformation, that favours agonist recruitment.

Altogether these data confirm that osmotic swelling modulates the β2-AR conformational landscape, favouring an active conformation that in turn leads to an enhanced downstream cAMP cascade.

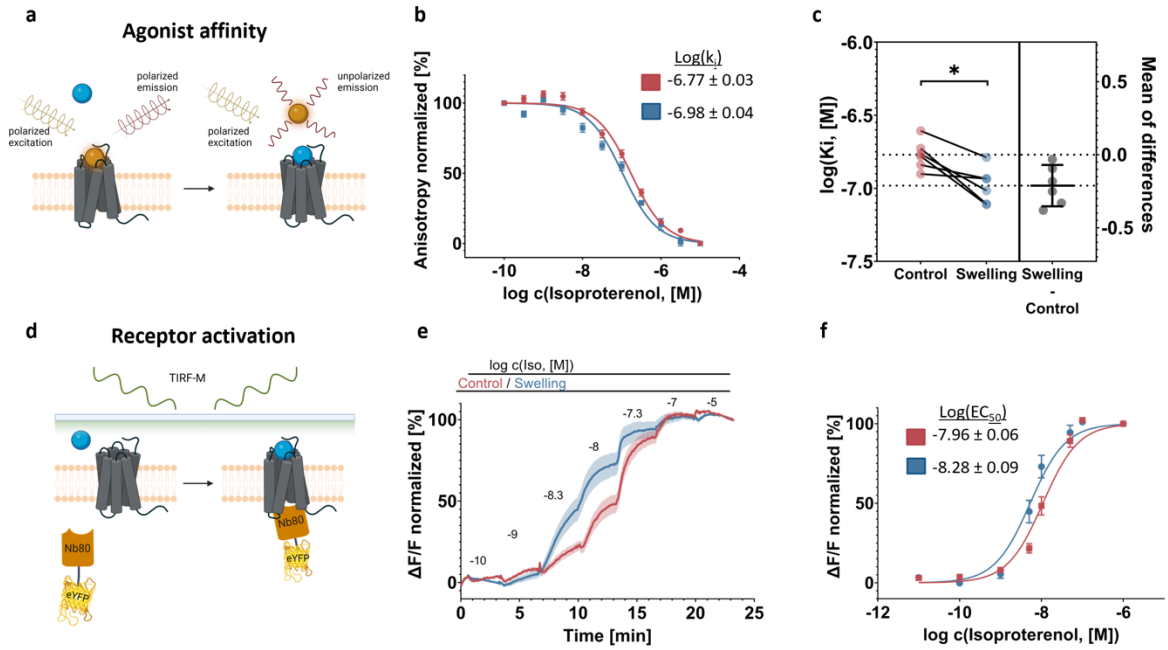

Figure 5 Swelling favors an active receptor conformation

a Ligand binding affinity is determined by employing a fluorescently labelled ligand and measuring the degree of fluorescence anisotropy; **b** average curve of increasing concentrations of isoproterenol displacing 2 nM of fluorescently labelled JE1319 from the β2-AR in swollen and non-swollen cells with the corresponding log(Ki) values; **c** pairwise comparison of log(Ki) values obtained from single experiments and the average of the difference overlay (for b and c - mean ± SEM; n = 6 plates from 5 independent experiments; statistical analysis by a paired two-tailed t-test); **d** conformational activation of the β2-AR is monitored by recruitment at the plasma membrane of the cell by employing the fluorescently tagged nanobody 80 (Nb80); **e** averaged time-sequence of the relative increase of membrane fluorescence collected as increasing concentrations of Iso are added to the cells (normalized to baseline and 10 μM Iso response); **f** the resulting averaged concentration response curves for cells in isotonic and swelling media and associated log(EC50) values (for e and f - mean ± SEM; n = 46 (control) and 45 (swelling) cells from 5 independent experiments).

Discussion

Our current understanding of the GPCR signaling cascade, from the ternary complex model down to the more recent structural determination of receptor conformational states, is facing a rapid and sustained evolution. Cartoons displaying GPCR signalling in textbooks still typically highlight only the receptor at the membrane, its ligand, and the downstream interaction partner, either the heterotrimeric G protein or, more frequently now, β-arrestins. However, literature reports indicate that GPCRs are exposed to many specific intracellular interactions with other proteins as well as to the modulatory effects of other, less described, interactions.

In particular, the intracellular domain of plasma membrane GPCRs is exposed to the cell cortex and its distinct organization[37]. In this work we decided to investigate a more general mechanism that can fundamentally alter the cortex and at the same time has a role in several (patho-)physiological processes, ranging from cardiac ischemia reperfusion[25] to renal function[38], namely osmotic swelling. In our hands, osmotic swelling became a tool to induce pleiotropic changes of the cortex and cell membrane, thereby affecting receptor function.

While osmotic swelling has been used before in the context of GPCR signaling[16,18], in these instances the GPCRs are observed to undergo activation upon pure mechanical stimulation. This is fundamentally different from our observations, that do not display spontaneous activation upon hypotonic shock at 200

mOsm, but only an effect upon additional agonist stimulation. Interestingly, the only report that discusses the ligand-dependent stimulation of a GPCR in cells undergoing osmotic swelling discusses the allosteric effect of hypotonic shock in favoring ligand-dependent recruitment of β-arrestin 2 to the AT1R[39], an effect we now also see for the β-ARs.

It shall be noted that we explore receptor function in the few minutes upon the onset of osmotic swelling, thus restricting the number of potential effects impacting the signalling cascade to rapid responses, arising from a local reorganization of the membrane and cortex (**Supplementary figure 8**), while excluding more lasting effects such as recruitment of phospholipids to the plasma membrane[40] or alterations to gene expression patterns[41]. On this timescale the overall curvature radius of the membrane decreases as the volume increases, while at the same time, small-scale ruffles on the plasma membrane, including caveolae, are 'flattened out' together with a remodulation of the actin cortex[40]. Caveolae are indeed recognised as important mediators of membrane mechanical response to external stresses[42] and their role in adrenergic signalling is also well established, especially in relation to β2-AR signalling[43]. Rasenick and colleagues reported that caveolae (disrupted by hyposmotic swelling) attenuate Gs signaling in response to isoproterenol. However, in their experiments, methyl-β-cyclodextrin (MβCD) treatment did not alter basal cAMP levels[44]. Osmotic swelling was further reported to specifically disrupt Caveolin1 – Gq protein interaction and attenuate Gq-mediated Ca^{2+} release[45]. In this work, the same effect on Gq signalling is observed upon cholesterol depletion under MβCD treatment, which leads to perturbation in caveolae structure. Interestingly, the same treatment was reported to increase beta-adrenergic mediated response to isoproterenol[46]. This would be in line with the observation that cell swelling leads to a reduction in number of caveolae [42]. Overall, there is thus a large and often conflicting mole of data on the effects of long-term/permanent modifications of membrane microdomains on GPCR signalling

On the backdrop of this scenario, we observe a significant increase in cAMP response in cells undergoing osmotic swelling, unaffected by MβCD disruption **(Supplementary Figure 5d)** . None of the previously mentioned works addressed the effects on cAMP caused by mild hypoosmotic swelling, which in our observations are transient. Moreover, our results show that a similar swelling-induced response is observed, besides the beta-AR system, also for receptors that are not traditionally associated to caveolae, such as histamine receptors or melanocortin receptors (**Supplementary Figure 1 F-H**).

We thus set out to dissect all steps of the β-AR signalling pathway in intact cells, to pinpoint where swelling is having an impact on the signalling cascade. In the course of our investigation we adapted and implemented a wide set of fluorescence spectroscopy techniques that allowed monitoring the activity of each of the signalling partners that support cAMP production and its regulation in single, living cells. Fluorescence cAMP biosensing allowed us to report on the effect (**Figure 1)** in HEK293 cells as well as in the more physiological setting of adult cardiomyocytes (**Figure 2**). This was then combined with specific drug combinations and knockout cell lines to rule out the role of trafficking (**Supplementary Figure 5b,h-j**), cAMP degradation (**Figure 3b and Supplementary Figure 5c**) or an altered activity of the ACs (**Figure 3c,d and Supplementary Figure 5 e-g**). Indeed, Fsk-induced AC activity appears unaffected by swelling in the absence of the G_s, suggesting that a key player in modulating the signalling cascade of the β-ARs is indeed the stimulatory heterotrimeric G protein. To further appreciate how G_s role in transducing receptor signalling is modulated upon osmotic swelling, we employed a fluorescent reporter for the active conformation of $G\alpha_s$, namely eYFP tagged Nb37, a nanobody originally developed to stabilize the structure of the active β2-AR in complex with $G\alpha_s$[47].

With this assay, we can then demonstrate that in swollen cells an equal concentration of agonist leads to an increased number of active receptor-$G\alpha_s$ complexes (**Figure 4a-c**), as well as an enhanced recruitment of β-Arrestin-2 (**Figure 4d-g**). These data may be explained either by the β-arrestin-2 wave following the successful recruitment and dissociation of of G_s at an increased number of receptors in swollen cells, or by osmotic swelling promoting a receptor active conformation that is non-selective of $G\alpha_s$ vs β-arrestin-2. Nonetheless, these results points to improved receptor to G protein coupling as the driving mechanism behind the observed increase in cAMP upon osmotic swelling. According to the ternary complex model[1], we thus investigated the possibility that osmotic swelling stabilizes the active

receptor conformation first by monitoring ligand binding in intact cells (**Figure 5a**) and then by a proxy for G protein coupling, namely the Nb80[36] (**Figure 5d**).

Upon ligand displacement experiments, the measured k_d displays a statistically significant change in swollen cells (**Figure 5b-c**), with increased affinity of the receptors towards isoproterenol in swollen cells. Moreover, the enhancement in Nb80 recruitment upon swelling displayed in **Figure 5e-f** corroborates the notion that a receptor active conformation is indeed favoured by osmotic swelling.

Overall, these results point to a modulation of receptor activity upon cell swelling, that we ascribe to cell swelling favouring the active conformation of the β2-AR. This observation would agree with a recent report suggesting that osmotic swelling leads to increased hydration of the intracellular side of the receptor, 'forcing open' the G protein binding pocket and thus favouring coupling[48]. Other explanations, such as an enhanced 'collision coupling' of the receptor to the G protein[49], are possible: while we observed a slight increase in receptor diffusion coefficients, we did not measure any increase in G protein ($G\alpha_s$) diffusion rate in swollen cells as opposed to control (**Supplementary Figure 9**). Since, as discussed, osmotic swelling has broad effects on the cell cortex and plasma membrane, such as actin remodelling, altered lipid composition, as well as changes in both local (flattening of ruffles and invaginations) and cell-wide (overall increase in volume) geometrical curvature[41], we believe it is difficult to pinpoint its effect to one specific molecular mechanism. However, the molecular mechanisms at play must directly scale with the osmolarity, as treatments with media of different osmolarity are observed to differentially affect cAMP concentrations, including a reduction of cAMP production by cell shrinkage (**Supplementary Figure 10**). Nonetheless, our observation with other G_s-coupled receptors as well as with the G_i coupled μOR, point to the generality of this regulatory mechanism.

These results suggest that osmotic cell volume changes can be intrinsic modulators of GPCR activity in several contexts of (patho-)physiological relevance, ranging from cardiac ischemia-reperfusion to the reported swelling of adipocytes[19]. In the heart such preference towards an active β2-AR state in swollen cells could potentially diminish the effect of antagonist administration. This is indeed what we observe: strikingly, in our measurements cell swelling leads to receptor activation by isoproterenol (as mimicked by Nb80 recruitment) even after an incubation with saturating concentration of propranolol, a prototypical β-blocker (**Supplementary Figure 6**).

Furthermore, cAMP has also been reported to be actively involved in cell volume regulation. It has been shown to support regulatory volume decrease in swollen cells[50] by additive stimulation of volume-regulated Cl^- efflux[51,52]. This may suggest an adaptive mechanism of swollen cells, that elevate normal agonist-dependent cAMP levels to favour return to normal volume.

Finally, membrane permeability for cAMP was shown to be increased upon osmotic swelling[53], potentially creating the need of increased production rate to compensate the efflux

Further studies and more refined biophysical approaches will be needed to deconvolve the specific molecular mechanisms mediating the effects of a pleiotropic perturbation such as osmotic swelling at the level of the isolated receptor. At the same time, additional functional investigations can shed light on the specific role of GPCR-mediated cAMP transient in the context of volume regulation and pathophysiological conditions like cardiac ischemia/reperfusion.

Materials and Methods

Cell culture. HEK293 and HEK293 derived cells (Epac-S^{H187} stable cell line, HEK293AD, $G\alpha_s$-KO cell line) were cultured in DMEM medium containing 4.5 g/l glucose (Gibco) supplemented with 10% fetal calf serum (FSC, Biochrome), 2 mM l-glutamine, 100 units/ml penicillin and 0.1 mg/ml streptomycin, at 37°C, 5% CO_2. To split cells, growth medium was removed by aspiration and cells were washed once with 10 mL of PBS (Sigma), followed by trypsinization for 2min in 1.5 mL of trypsin 0.05%/EDTA 0.02% (PAN Biotech) solution and resuspended in the desired amount of DMEM medium.

Transfection. For the single cell microscopy experiments the cells were transfected directly in the imaging dishes 24 hours prior to conducting the experiments, using JetPrime transfection reagent

(Polyplus) according to manufacturer's protocol. For the plate reader experiments the cells were transfected on 10 cm plates 48 hours before the experiment using a reduced amount of JetPrime transfection reagent and total DNA (5 µl and 2.5 µg respectively) and transferred to black 96-well plates (Brandt) 24 hours before the experiment. The transfected cDNA and cDNA ratios for co-transfections are listed in further sections.

Molecular cloning. The tricistronic G_s and G_s-CFP plasmids were created using NEBuilder HiFi DNA assembly cloning kit (NEB). $G\alpha_s$ (or $G\alpha_s$-CFP[54]), $G\beta_1$ and $G\gamma_2$ were cloned into the pcDNA3(+) backbone following the same structure as for the published G_i FRET sensors [23]: $G\beta_1$-2A-$G\gamma_2$-IRES-$G\alpha_s$ (or $G\alpha_s$-CFP respectively).

Swelling medium. Throughout all experiments two types of imaging buffers (control – mannitol electrolyte solution 300 mOsm (MES300) and swelling – mannitol electrolyte solution 200 mOsm (MES200)) were used. A basic buffer with a low osmolarity – ES150 – was produced by solving 60 mM NaCl, 5 mM KCl, 2 mM $CaCl_2$, 1 mM $MgCl_2$, 10 mM HEPES in distilled water and resulting in electrolyte solution 150 mOsm (ES150). It was then supplemented with 150 mM mannitol (Sigma) to produce MES300 and reach 300 mOsm. MES300 was then used for washing and incubation steps as described in specific experiments. To achieve hypotonic conditions of 200 mOsm during the experiments, 2/3 of the total volume of MES300 was removed from the wells and replaced with the same volume of ES150, resulting in MES200. In control condition 2/3 of MES300 were also removed and replaced with fresh MES300 to avoid ascribing any effects to mechanical artifacts.

Cardiomyocyte isolation. Cardiomyocyte isolation involved obtaining cardiac myocytes from adult ventricles of CAG-Epac1-camps mice aged 8 to 12 weeks[9], regardless of their gender. The process employed enzymatic collagen digestion and retrograde perfusion through the aorta using a Langendorff perfusion apparatus, as previously described[9]. In brief, the hearts were swiftly removed from the mice after cervical dislocation and connected to a custom-built perfusion system. Initially, the hearts were perfused with perfusion buffer for 4 minutes at a rate of 3 ml/min, followed by an 8-minute perfusion with myocyte digestion buffer containing 5 mg of liberase dispase high DH enzyme (Roche) per digestion. Subsequently, the heart was detached from the perfusion system, and the ventricles were dissected into small pieces using scalpels. After sedimentation, removal of the supernatant, and resuspension the cells were filtered through a nylon mesh cell strainer (100 µm pore size, Falcon) to eliminate any remaining tissue fragments. The cells were then gradually exposed to physiological Ca^{2+} concentrations (~1 mM), resuspended in myocyte plating medium, and seeded on freshly coated Matrigel-coated 8-well Ibidi µ-slides for each experiment. More detailed information about the buffers and materials used can be found in the methods section of Bathe-Peters et al[9].

Cell area measurements with confocal microscopy. To measure the effect of hypotonic treatment on cell area murine cardiomyocytes were seeded in 8-well Ibidi µ-slides with a density of 1,000 cells per well and labeled with Cell Mask™ Deep Red according to manufacturer's protocol. XY and XZ movies of cells were then acquired on a confocal laser scanning microscope, Leica SP8, with a white-light laser at the wavelength of 633 nm and laser power of 5%. All measurements were conducted with an HC PLAP CS2 40×1.3 numerical aperture (NA) oil immersion objective (Leica). Movies were acquired at 30 seconds per frame with a hybrid detector in the range of 643 to 693 nm. Medium change to induce swelling was performed as described in previous sections. ImageJ was used to conduct thresholding and object detection on the cells and the extracted area was plotted with GraphPad Prism v. 9.5.1.

Linescan measurements with confocal microscopy. HEK293AD cells were seeded in 8-well Ibidi® µ-slides with a density of 25,000 cells per well and transfected with 0,25 µg Gαs-eYFP using the JetPrime® transfection kit according to manufacturer's protocol. Linescans were conducted in a SP8 confocal microscope (Leica Microsystems) and analyzed as previously described[55].

FRET microscopy. HEK293 cells stably expressing Epac-S^{H187} sensor were seeded in 8-well Ibidi µ-slides with a density of 25,000 cells per well. Cells were washed twice in MES300 and imaged at room temperature. An inverted microscope (DMi8, Leica Microsystems), equipped with an x63 HC PL APO, 1.40-0.60 numerical aperture (NA) objective (Leica Microsystems), dichroic beamsplitter T505lpxr (Visitron Systems), xenon lamp coupled with a continuously tunable Visichrome high-speed

polychromator (Visitron Systems) and a metal-oxide-semiconductor camera (Prime95B, Teledyne Photometrics) with a dual image splitter (OptoSplit II, Cairn Research), was used. Excitation wavelength of 445 nm was used, and fluorescence emission was simultaneously recorded at 470/24 nm and 535/30 nm. The movies were obtained at 5 seconds per frame for the number of frames needed for the cAMP concentrations to equilibrate. ImageJ was used to extract fluorescence intensity values from single cells, which were corrected for background and used to calculate FRET/CFP ratio.

Plate reader cAMP FRET measurements. HEK293 cells stably expressing Epac-S^{H187} sensor were seeded in black 96-well plates (Brand) with a density of 50,000 cells per well. $G\alpha_s$-KO cells were transfected with either 2.5 µg Epac-S^{H187} or with 1.25 µg Epac-S^{H187} plus 1.25 µg $G\alpha_s$ 24 h prior to seeding in 96-well plates. 24 h after seeding cells were washed twice with 90µl MES300 per well. After 5min incubation at 37°C, baseline measurement was conducted in a Neo2 plate reader (Biotek) using 420 nm excitation and 485nm / 540nm emission filters. As the second step, 60 µl MES300 were removed from each well and replaced with 60µl of either MES300 or ES150 for the “control” and “swelling” conditions respectively and the plate was measured for 15 minutes. Afterwards the desired dilution series with increasing concentrations of ligand was added (10 µl per well of a 10x concentration in MES300) and the plate was measured again for 15 minutes. At last, a mix of forskolin/IBMX in MES300 was added to an end concentration of 10 µM forskolin and 100 µM IBMX and measured for 10 more minutes. The change in acceptor/donor ratio was normalized to 0% baseline and 100% forskolin/IBMX and plotted in GraphPad Prism v.9.5.1. For the concentration response curves “Dose-response stimulation fit (three parameters)” was applied.

TIRF microscopy. HEK293AD cells were seeded in 8-well Ibidi® µ-slides with a density of 25,000 cells per well and transfected with JetPrime® transfection according to manufacturer’s protocol. Following cDNA amounts per well were used: for Nb80 recruitment – 0.225 µg Snap-ß2AR and 0.025 µg Nb80-eYFP; for Nb37 recruitment – 0.05 µg Snap-ß2AR, 0.15 µg $G\beta_1$-2A-$G\gamma_2$-IRES-$G\alpha_s$ and 0.05 µg Nb37-eYFP; Transfected cells were labeled with 1 µM SNAP-Surface 674 dye (NEB) for 30min followed by washing two times for 10 min with 300 µl MES300 per well. After labeling, cells were subsequently taken for imaging to an Attofluor cell chamber (Fisher Scientific) in MES300. A TIRF illuminated Eclipse Ti2 microscope (Nikon), equipped with a x100, 1.49 NA automated correction collar objective and 405-, 488-, 561-, 647-nm laser diodes coupled via an automated N-Storm module and four iXon Ultra 897 EMCCD cameras (Andor), was used. Objective and cell chamber were kept at 37°C during imaging. The automated objective collar was on, and hardware autofocus was activated. Movies were acquired at 4s per frame for 400 frames. After a baseline measurement of 50 frames increasing concentrations of isoproterenol were added to the imaged well in 50 frame steps. Prior to each isoproterenol addition 30 µl of solution was removed from the well and 30 µl of 10x isoproterenol in either MES300 or MES200 was applied. ImageJ was used to extract fluorescence intensity values, which were corrected for background and normalized to 0% baseline and 100% 10µM isoproterenol stimulation. In case of F-actin content measurement HEK293AD cells were transfected with Lifeact-eGFP and imaged as described above at 30 seconds per frame.

Single-molecule TIRF microscopy. HEK293AD cells were seeded on glass coverslips in 6-well plates at a density of 250,000 cells per well. To ensure low levels of receptor expression, necessary for single-particle imaging, transfection with 2 µg Snap-β2AR was performed with the JetPrime® transfection kit 3-4 hours before imaging. SNAP-tagged receptors were labelled with 1µM SNAP-surface 549® dye and washed twice for 15 minutes with the imaging buffer (MES300). Imaging was done using AttoFluor chambers with the objective and the sample kept at 20°C. The movies of receptor diffusion were then recorded via the Cy3 emission channel under illumination by the 561 nm laser at 100% laser power. Exposure time was set to 30 ms and movie length limited to 1000 frames to avoid excessive photobleaching.

Single particle tracking analysis. Obtained TIRF movies were analyzed by uTrack software[56], loaded to the MATLAB environment. Point source detection and tracking analysis (incl. segment merging/splitting; maximum gap to close – 1 frame) modules were executed and resulting files, containing movie trajectories were loaded to MATLAB. Trajectories were filtered by length (between 3 and 100 frames) and by a manually defined ROI, selecting basolateral membranes of the cells. Mean square displacements for each movie were calculated over a time lag of 100 frames. A linear regression

was fit to the first five frames of every resulting MSD movie and the slope was divided by four to obtain the diffusion coefficient.

Plate reader ligand binding assays. HEK293 cells were seeded in 10 m culture plates, co-transfected with 0.5 µg Snap-ß2AR, 0.5 µg Nb37-eYFP and 1.5 µg $G\beta_1$-2A-$G\gamma_2$-IRES-$G\alpha_s$-CFP after 24 h and reseeded in black 96-well plates with a density of 50,000 cells per well another 24 h later. The plate was incubated with 100ul MES300 containing 2nM JE1319. As the second step, 60 µl MES300 was removed from each well and replaced with 60µl of either MES300 or ES150 (both containing 2nM JE1319) for the "control" and "swelling" conditions respectively and the plate was incubated for further 15 minutes. Afterwards the desired dilution series with increasing concentrations of isoproterenol was added (10 µl per well of a 10x concentration in MES300) and the plate was incubated for 90 minutes and measured in a Neo2 plate reader (Biotek) using DualFP polarization filter and an 620nm/680 nm excitation/emission filter. A G-factor of 0.12 was measured for the instrument. Fluorescence anisotropy was calculated as $r = (I_{\parallel} - I_{\perp})/(I_{\parallel} + 2I_{\perp})$ and plotted in GraphPad Prism v.9.5.1. For the concentration response curves "Dose-response inhibition fit (three parameters) was applied with min and max being constrained to 0% and 100% respectively.

Plate reader G_i-FRET sensor assay. HEK293 cells were seeded in 10cm cell culture dishes at a density of 4×10^6. Cells were co-transfected with 0.5µg SNAP-µOR and 2µg G_{i2} FRET sensor 24h after seeding, as described in previous sections; 24 h after transfection, cells were trypsinized and transferred into black 96-well plates (Brand), at a density of 50,000 cells per well; 16 h to 24 h later, cells were washed with MES300, and then 90 µl of MES300 was added to each well. After 10min incubation at 37°C, measurement was performed at 37°C using a Synergy Neo2 Plate Reader (Biotek) using a CFP/YFP FRET filter set. After basal FRET measurement, medium was changed as described above and after 15 minutes of further measurement 10 µl of ligand solution were applied to each well. The change in acceptor/donor ratio was normalized to 0% baseline and plotted in GraphPad Prism v.9.5.1. For the concentration response curves "Dose-response stimulation fit (three parameters)" was applied.

AlphaScreen cAMP detection assay. HEK293 cells were seeded in transparent 96-well plates (TPP) at a density of 25,000 cells per well. After 24h the growing medium was exchanged to 100µ of either MES300 or MES200 and increasing concentrations of isoproterenol were added to corresponding wells. After 10 minutes of stimulation, the plate was frozen at -80°C for 15 minutes, resulting in cell lysis. The contents of the plate were then thawed at room temperature and 10µl from each well were respectively transferred to a 384-well white OptiPlate™ plate (Revvity). cAMP standard solutions, acceptor- and donor-bead solutions were prepared and added to the plate according to the manufacturer's protocol. The readouts of fluorescence intensity were performed at a VICTOR Nivo™ plate reader (Revvity) according to a measurement protocol provided by the manufacturer. The resulting cAMP concentrations were calculated and plotted in GraphPad Prism v.10.2.1. For the concentration response curves "Dose-response stimulation fit (three parameters)" was applied.

Acknowledgments

This project was supported by the Deutsche Forschungsgemeinschaft (DFG), via collaborative research center 1423 Project 421152132, Subproject C03 (to P.A. and M.J.L.).

We are grateful to Bärbel Pohl, Marlies Grieben and Ulrike Zabel for their excellent technical assistance. We would like to acknowledge Heike Biebermann (Charité UniversitätsMedizin, Berlin) for kindly sharing the HEK293 cells stably expressing Epac1-S^{H187}, and Peter Gmeiner (Friedrich-Alexander-Universität, Erlangen) for synthetizing the ligand JE1319. Nb80 and Nb37 plasmids were a gift from Mark von Zastrow (UCSF). Epac1-S^{H187} biosensor plasmid was a gift from Kees Jalink (The Netherlands Cancer Institute, Amsterdam). We are grateful to Romy Thomas (Max Delbrück Center, Berlin) for helping us generate the tricistronic heterotrimeric G protein expression vector used in our experiments.

Author contributions

A.S. and P.A. designed research; A.S. performed research; A.I. contributed new reagents/analytic tools; A.S. and P.A. analyzed data; M.B.-P. supported the preparation of primary cardiomyocytes; P.A and

M.J.L. supervised the project and acquired funding; P.A. and A.S. wrote the paper with input from all authors.

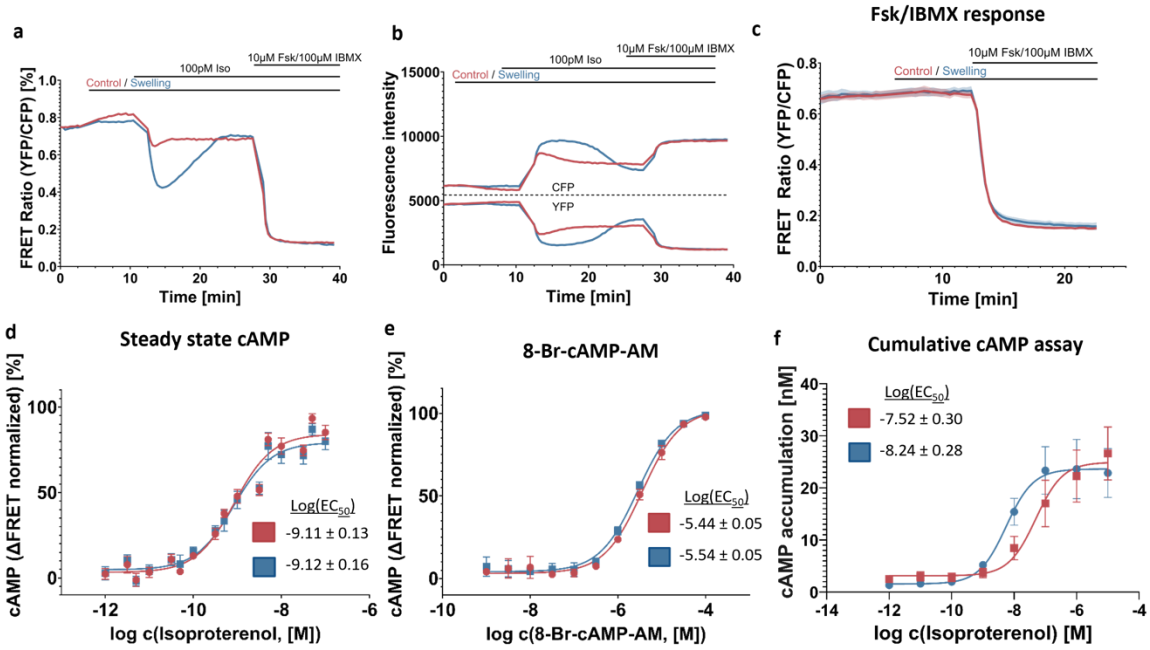

Supp. Fig. 1: Effect of swelling on receptor signaling is not caused by sensor artifacts.
a,b non-normalized FRET ratio (**a**) and respective CFP and YFP channel traces (**b**) for the representative curve showed in the main **Fig. 1 c**; **c** average normalized kinetic curves of acceptor/donor ratio measured at baseline, after medium change to control or swelling medium and after addition of 10µM Forskolin + 100µM IBMX (mean ± SEM; n = 3 independent experiments); **d** averaged concentration response curves representing steady state cAMP concentrations as indicated in **Fig. 1 c** (mean ± SEM; n = 3 independent experiments); **e** averaged concentration response curves of HEK293 Epac-SH187 stable cell line being stimulated by increasing concentrations of 8-Br-cAMP-AM (normalized to baseline and 10µM forskolin + 100µM IBMX; mean ± SEM; n = 3 independent experiments); **f** concentration-response curves obtained by measuring cAMP concentrations with the AlphaScreen endpoint cAMP assay in cell lysates of untransfected HEK293T cells, that were incubated in an isotonic and hypotonic medium containing indicated concentrations of isoproterenol for 10 minutes prior to cell lysis (mean ± SEM; n = 12 replicates from 4 independent experiments).

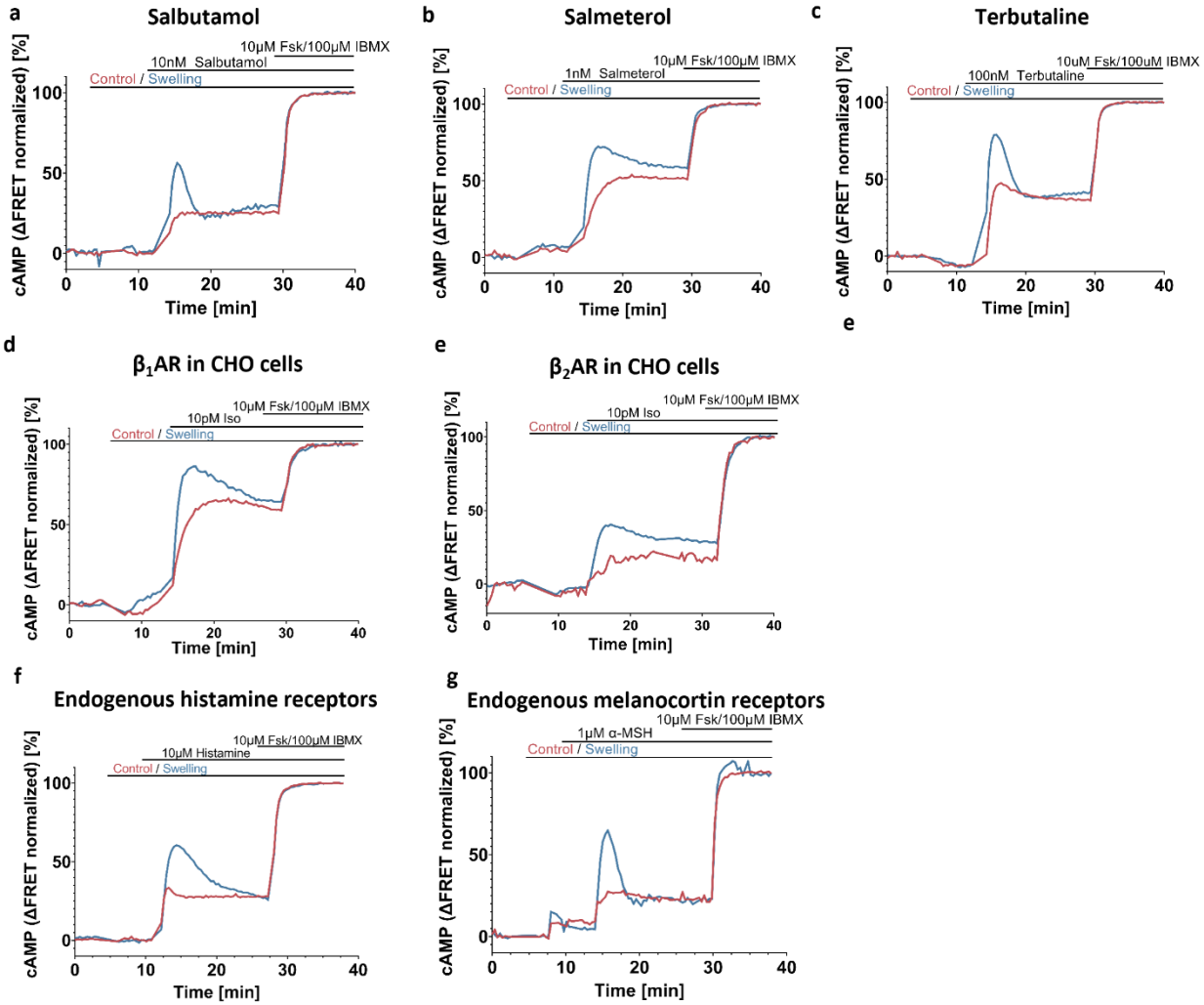

Supp. Fig. 2: Effect of swelling on receptor signaling is generalizable to other β-AR agonists, β-AR subtypes and to other Gs-coupled GPCRs.

a-c representative curves showing kinetic cAMP concentrations as a response to different β-adrenergic agonists in HEK293 Epac-S^{H187} stable cells (normalized to baseline and 10μM Forskolin + 100μM IBMX); **d,e** representative curves of intracellular cAMP concentration upon stimulation with 10 pM isoproterenol of CHO cells transfected with Snap-β1AR (or Snap-β2AR for **e**) and Epac-S^{H187} sensor; **f,g** representative curves showing kinetics cAMP concentrations as a response to histamine (**f**) and α-MSH (**g**) in HEK293 Epac-SH187 stable cells (normalized to baseline and 10μM forskolin + 100μM IBMX);

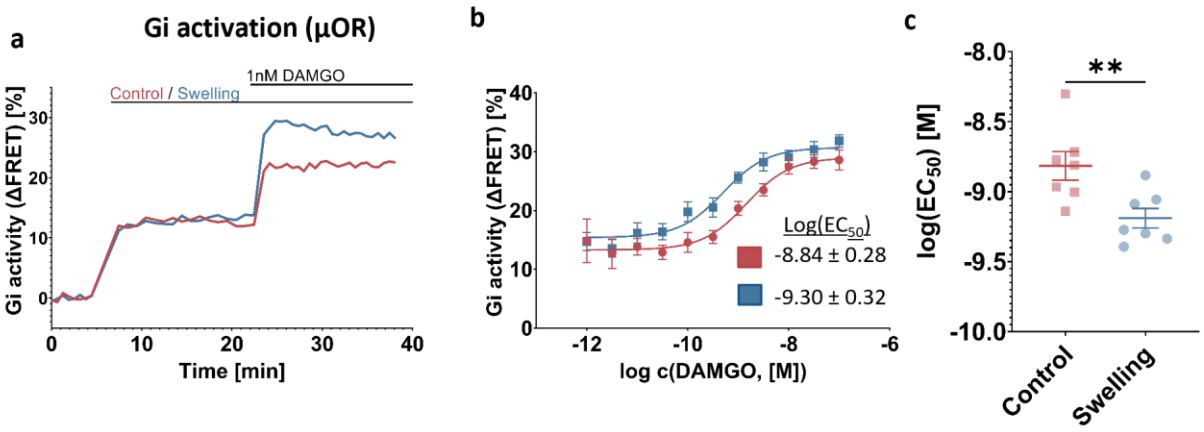

Supp. Fig. 3: Effect of swelling on receptor signaling is generalizable also to G_i-coupled receptors.

a-c Representative curve (**a**), averaged concentration response curve (**b**) and log(EC_{50}) values from individual experiments (**c**) comparing G_{i2} FRET-sensor response to DAMGO in control and swollen HEK293 cells, transiently transfected with µOR and the G_{i2}-FRET sensor.

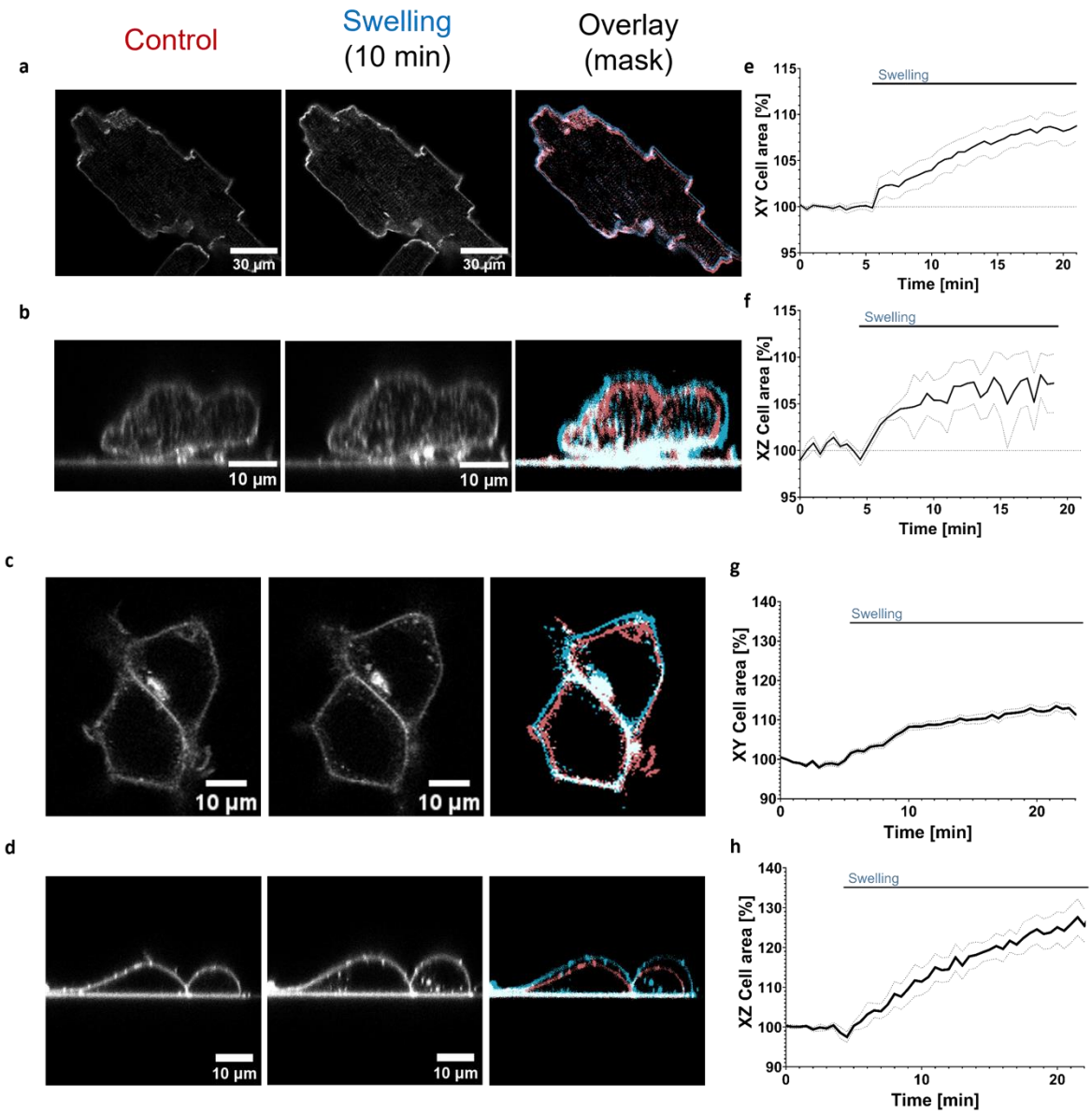

Supp. Fig. 4: Characterization of cardiomyocyte and HEK293 swelling

a-d Confocal images of cardiomyocytes (**a,b**) and HEK293 cells (**c,d**) under isotonic conditions (left) and after 20 minutes of exposure to swelling medium (middle), with an overlay of cell edges under both conditions (right; isotonic in red and swelling in blue). **a** and **c** show XY projections, while **b** and **d** show cells in a XZ projection; **e-h** average area changes over time for cardiomyocytes (**e,f**) and HEK293 cells (**g,h**) in the XY and XZ projections respectively (mean ±SEM, n = 6 cells from 3 independent experiments (**e**), 3 cells from 2 experiments (**f**), 33 cells from 3 experiments (**g**) and n = 7 cells from 3 experiments (**h**)).

Supplementary movie 1 (cAMP in CM upon Iso and Fsk/IBMX stimulation)

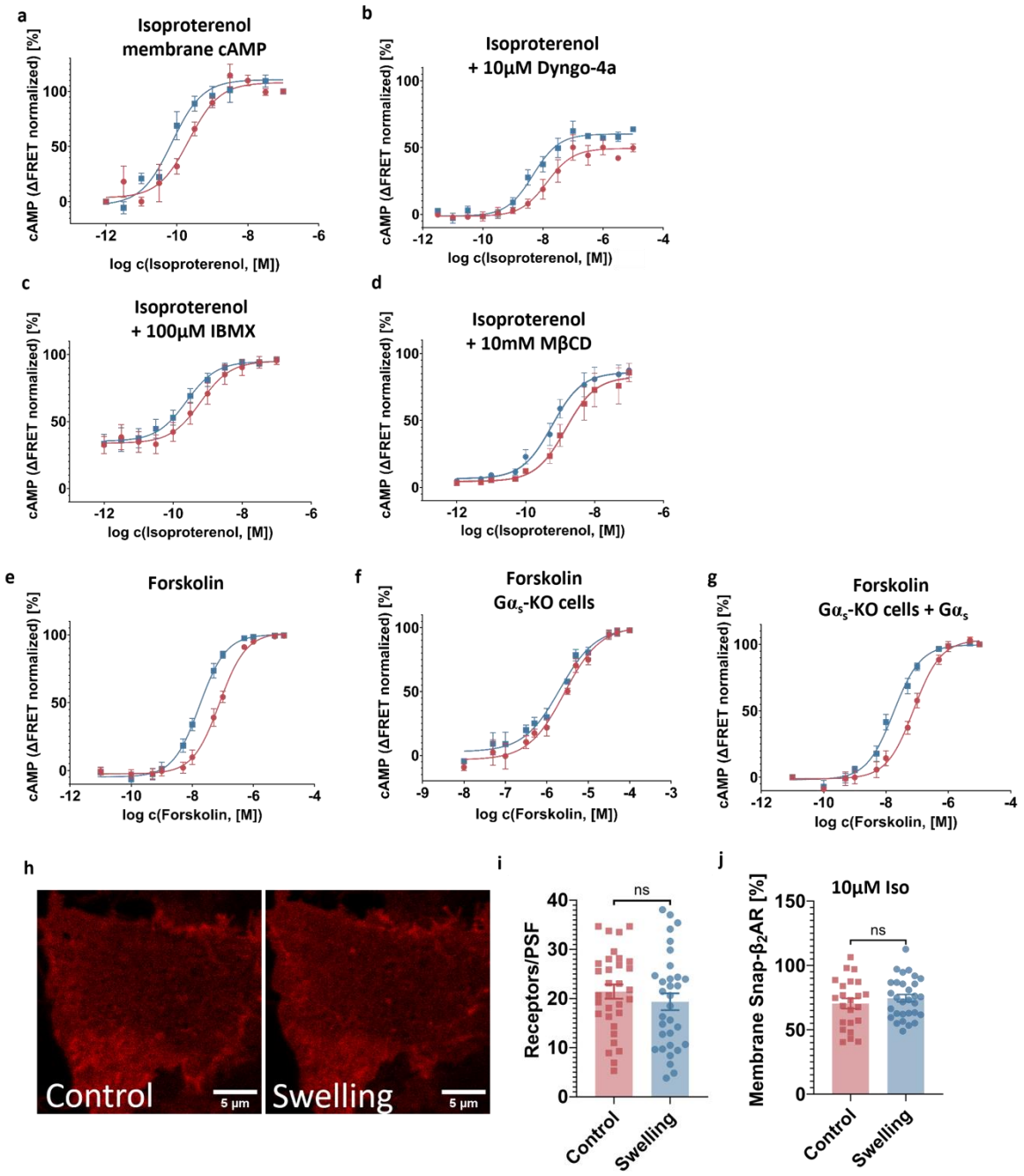

Supp. Fig. 5: Impact of cell swelling on isoproterenol potency under selective regulation of the β-adrenergic signalling cascade

a-g Averaged concentration response curves of intracellular cAMP concentrations under following conditions: (**a**) local cAMP at the plasma membrane upon Iso stimulation measured with an Epac1-Camps-CAAX sensor (transiently transfected HEK293 cells); (**b**) cytosolic cAMP measured upon Iso stimulation after treatment with 10 µM Dyngo4a for 30 min (HEK293 Epac-S^{H187} stable cell line); (**c**) cytosolic cAMP measured upon Iso stimulation with simultaneous addition of 100µM IBMX (HEK293 Epac-S^{H187} stable cell line); (**d**) cytosolic cAMP measured upon Iso stimulation after treatment with 10 mM methyl-β-cyclodextrine for 30 min (HEK293 Epac-S^{H187} stable cell line); (**e,f,g**) cytosolic cAMP measured upon forskolin stimulation in (**e**) wt $G\alpha_s$ phenotype (HEK293 transfected with Epac-S^{H187}), (**f**) $G\alpha_s$-KO cells (transfected with Epac-S^{H187}) and (**g**) $G\alpha_s$-KO cells transiently transfected with $G\alpha_s$ and Epac-S^{H187}; **h** representative confocal images of basolateral membrane of HEK293AD cell transiently transfected with Snap-β2AR and labelled with SnapSurface-Alexa674 dye before and after hypotonic treatment; **i** number of receptors per pixel as obtained from single cells before and after hypotonic treatment (paired two-tailed t-test; mean ± SEM; n = 32 cells from 4 independent experiments); **j** relative

number of receptors at the plasma membrane (compared to baseline) after 10 min of 10µM isoproterenol stimulation (paired two-tailed t-test; mean ± SEM; n = at least 23 cells from 3 independent experiments).

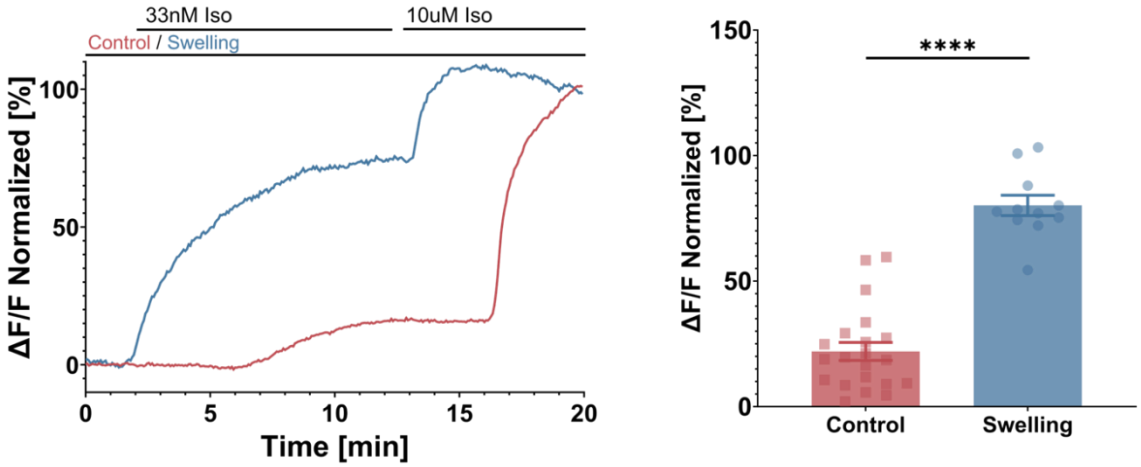

Supp. Fig. 6: Swelling leads to an increased β-arrestin2 recruitment independent of $G\alpha_s$
a representative curve showing relative increase of membrane fluorescence collected as first 33 nM, and then at saturating 10 µM concentration of isoproterenol is added to the cell (normalized to baseline and 10 µM Iso response); **b** relative fluorescence increase measured upon β-arrestin2-eYFP recruitment upon 33 nM isoproterenol stimulation in swollen vs non-swollen cells (mean ± SEM; n = 21 (control) and 1 (swelling) cells from 3 independent experiments; statistical analysis performed by an unpaired two-tailed t-test).

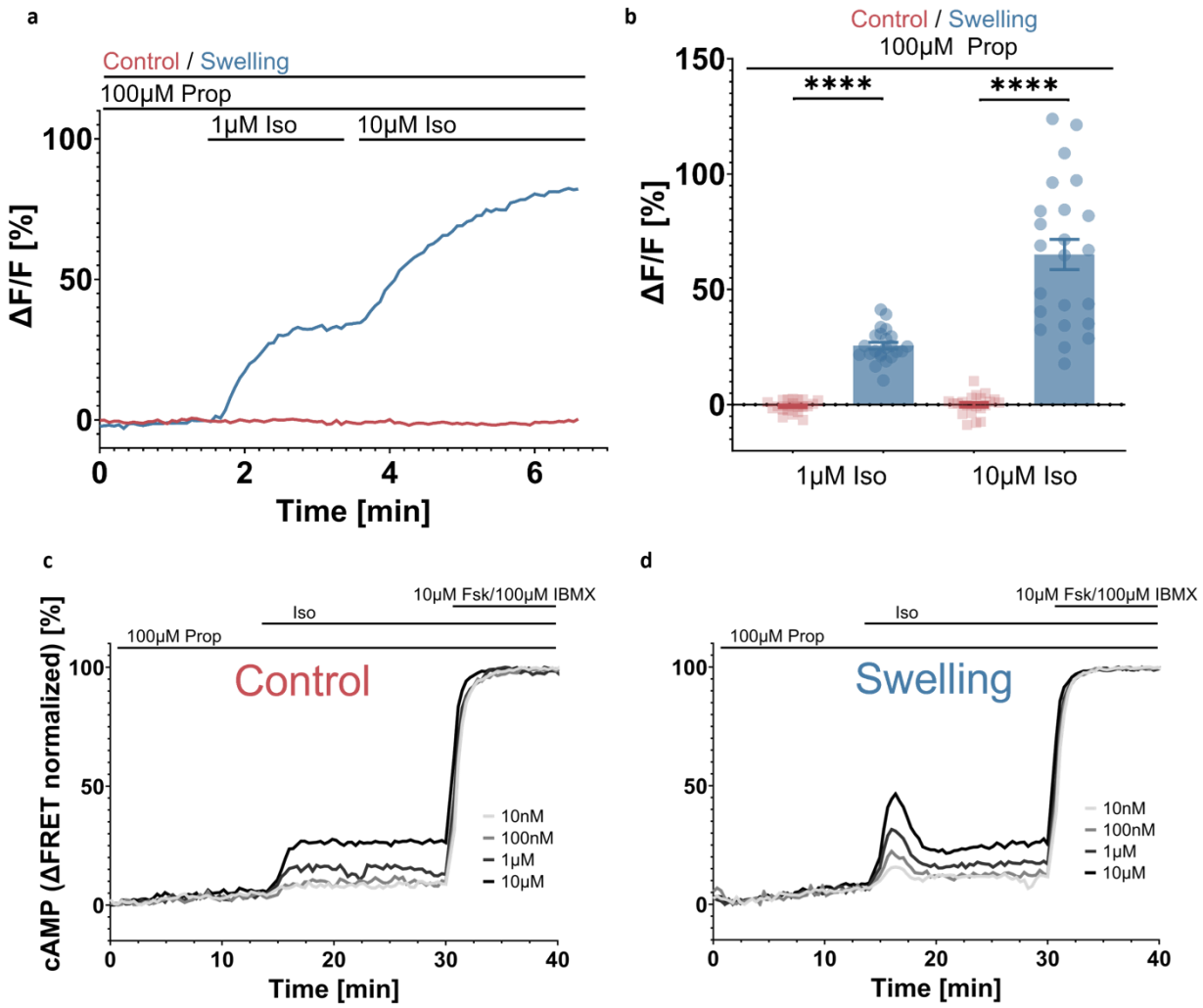

Supp. Fig. 7: Swelling reduces propranolol blocking efficiency of β2-AR

a Representative time-sequence of the relative increase of Nb80-eYFP fluorescence signal at the basolateral membrane, as isoproterenol is added after 60 min incubation with 100 µM propranolol; **b** relative fluorescence increase measured upon Nb80-eYFP recruitment upon 1 µM and 10 µ M isoproterenol stimulation in swollen vs non-swollen cells (mean ± SEM; n = at least 21 cells from 3 independent experiments; statistical analysis performed by an unpaired two-tailed t-test); **c, d** representative kinetic curves of acceptor/donor ratio measured in HEK293T cells stably expressing Epac-S^{H187} in a microplate reader after 1h preincubation with 100µM propranolol and consecutive addition of indicated isoproterenol concentrations; cells were additionally incubated in control (**c**) or swelling (**d**) medium, containing 100µM propranolol, before isoproterenol addition.

Supplementary movie 2 (Nb37-eYFP recruitment)

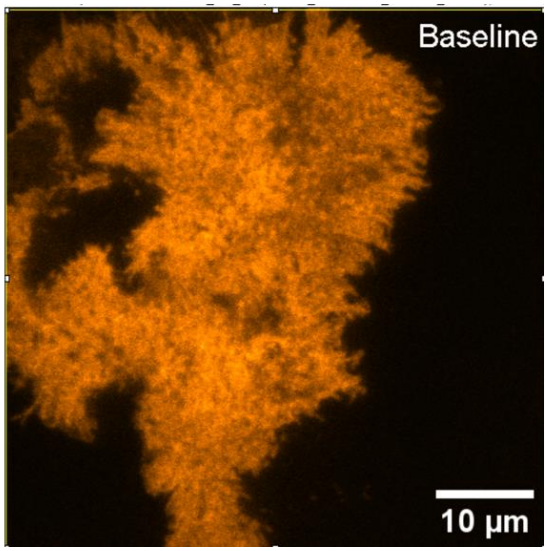

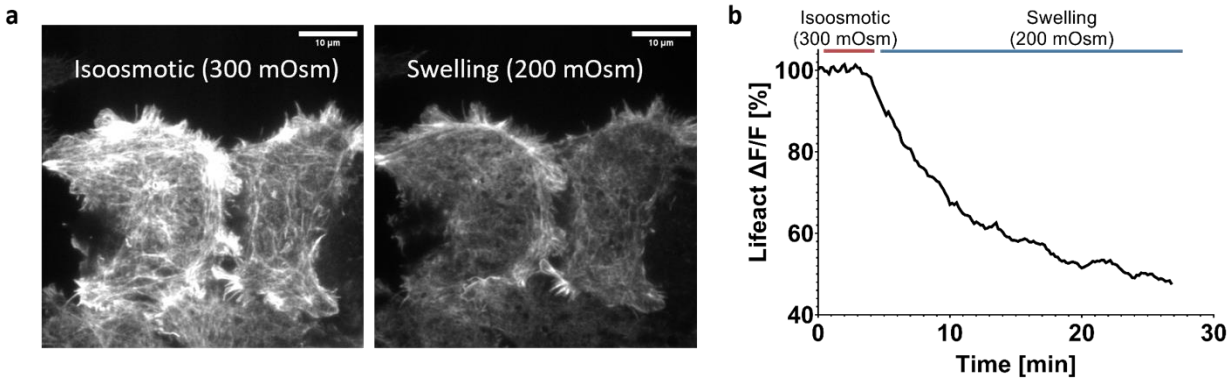

Supp. Fig. 8: F-actin labelling shows a decrease in cortical actin polymerization upon induction of cell swelling

a Representative TIRF-M images of HEK293AD cells transfected with Lifeact-eGFP and visualizing F-actin in basal conditions (left) and after 20 minutes of incubation in swelling medium (right) b quantification of Lifeact-eGFP intensity over the course of time for one representative cell.

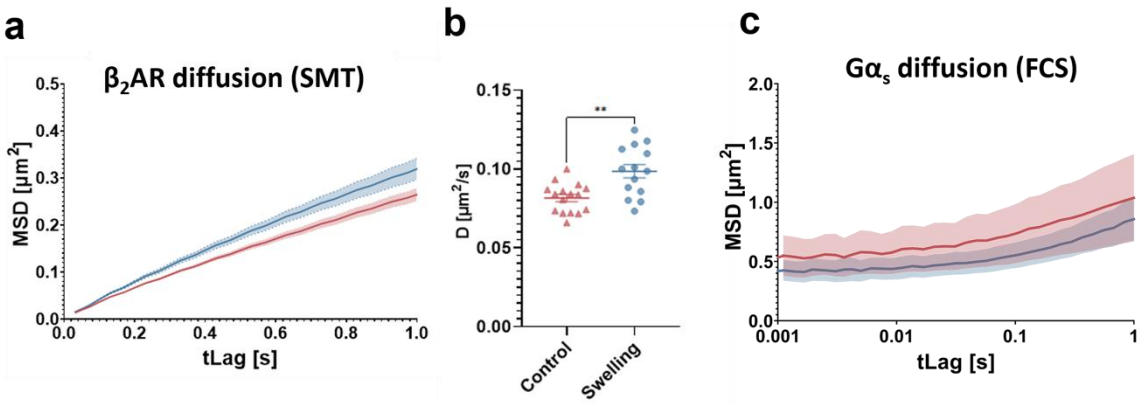

Supp. Fig. 9: Single molecule tracking shows faster ß2AR plasma membrane diffusion in swollen cells

a averaged mean squared displacement curves obtained by tracking Snap-ß2AR diffusing on basolateral membrane of transiently transfected HEK293AD cells using TIRF-M; **b** diffusion coefficients calculated per cell from the first 0.15 s of corresponding MSD plots (MSD = 4Dt) (mean ± SEM; n = 16 (control) and 14 (swelling) cells from 3 independent experiments; statistical analysis by an unpaired t-test); **c** averaged mean squared displacement curves obtained by tracking $G\alpha_s$-eYFP diffusing on basolateral membrane of transiently transfected HEK293AD cells using confocal microscopy-based linescan FCS (mean ± SEM; n = at least 7 cells from 2 independent experiments).

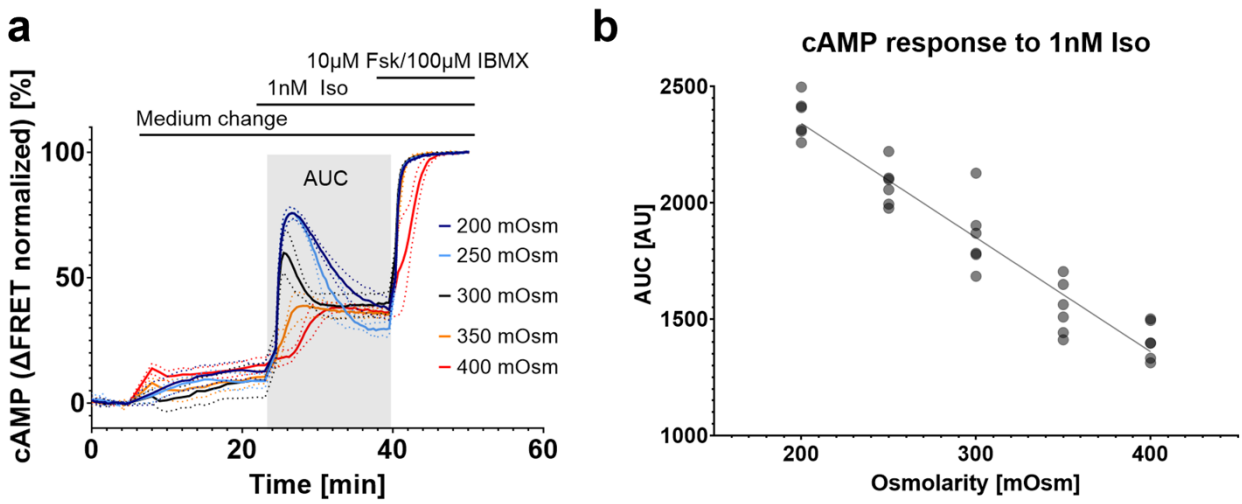

Supp. Fig. 10: Osmolarity can be titrated to differentially modulate cAMP production

a averaged curves of intracellular cAMP concentration under different osmolarities; **b** areas under the curve obtained from single experiments and plotted against osmolarity, including a linear regression fit (n = 6 plates from 2 independent experiments).

References

1 De Lean, A., Stadel, J. M. & Lefkowitz, R. J. A ternary complex model explains the agonist-specific binding properties of the adenylate cyclase-coupled beta-adrenergic receptor. *J Biol Chem* **255**, 7108-7117 (1980).

2 Shukla, A. K., Singh, G. & Ghosh, E. Emerging structural insights into biased GPCR signaling. *Trends Biochem Sci* **39**, 594-602 (2014). https://doi.org:10.1016/j.tibs.2014.10.001

3 Leach, K., Sexton, P. M. & Christopoulos, A. Allosteric GPCR modulators: taking advantage of permissive receptor pharmacology. *Trends Pharmacol Sci* **28**, 382-389 (2007). https://doi.org:10.1016/j.tips.2007.06.004

4 Hay, D. L., Poyner, D. R. & Sexton, P. M. GPCR modulation by RAMPs. *Pharmacol Ther* **109**, 173-197 (2006). https://doi.org:10.1016/j.pharmthera.2005.06.015

5 Oates, J. & Watts, A. Uncovering the intimate relationship between lipids, cholesterol and GPCR activation. *Curr Opin Struct Biol* **21**, 802-807 (2011). https://doi.org:10.1016/j.sbi.2011.09.007

6 Cao, T. T., Deacon, H. W., Reczek, D., Bretscher, A. & von Zastrow, M. A kinase-regulated PDZ-domain interaction controls endocytic sorting of the beta2-adrenergic receptor. *Nature* **401**, 286-290 (1999). https://doi.org:10.1038/45816

7 Soubias, O., Teague, W. E., Hines, K. G. & Gawrisch, K. The role of membrane curvature elastic stress for function of rhodopsin-like G protein-coupled receptors. *Biochimie* **107 Pt A**, 28-32 (2014). https://doi.org:10.1016/j.biochi.2014.10.011

8 Rosholm, K. R. *et al.* Membrane curvature regulates ligand-specific membrane sorting of GPCRs in living cells. *Nat Chem Biol* **13**, 724-729 (2017). https://doi.org:10.1038/nchembio.2372

9 Bathe-Peters, M. *et al.* Visualization of beta-adrenergic receptor dynamics and differential localization in cardiomyocytes. *Proc Natl Acad Sci U S A* **118** (2021). https://doi.org:10.1073/pnas.2101119118

10 Calebiro, D. *et al.* Persistent cAMP-signals triggered by internalized G-protein-coupled receptors. *PLoS Biol* **7**, e1000172 (2009). https://doi.org:10.1371/journal.pbio.1000172

11 Kockelkoren, G. *et al.* Molecular mechanism of GPCR spatial organization at the plasma membrane. *Nat Chem Biol* **20**, 142-150 (2024). https://doi.org:10.1038/s41589-023-01385-4

12 Ostrom, R. S. & Insel, P. A. The evolving role of lipid rafts and caveolae in G protein-coupled receptor signaling: implications for molecular pharmacology. *Br J Pharmacol* **143**, 235-245 (2004). https://doi.org:10.1038/sj.bjp.0705930

13 Romero, G., von Zastrow, M. & Friedman, P. A. Role of PDZ proteins in regulating trafficking, signaling, and function of GPCRs: means, motif, and opportunity. *Adv Pharmacol* **62**, 279-314 (2011). https://doi.org:10.1016/B978-0-12-385952-5.00003-8

14 Scarselli, M. *et al.* Revealing G-protein-coupled receptor oligomerization at the single-molecule level through a nanoscopic lens: methods, dynamics and biological function. *FEBS J* **283**, 1197-1217 (2016). https://doi.org:10.1111/febs.13577

15 Hardman, K., Goldman, A. & Pliotas, C. Membrane force reception: mechanosensation in G protein-coupled receptors and tools to address it. *Current Opinion in Physiology* **35** (2023). https://doi.org:10.1016/j.cophys.2023.100689

16 Chachisvilis, M., Zhang, Y. L. & Frangos, J. A. G protein-coupled receptors sense fluid shear stress in endothelial cells. *Proc Natl Acad Sci U S A* **103**, 15463-15468 (2006). https://doi.org:10.1073/pnas.0607224103

17 Zou, Y. *et al.* Mechanical stress activates angiotensin II type 1 receptor without the involvement of angiotensin II. *Nat Cell Biol* **6**, 499-506 (2004). https://doi.org:10.1038/ncb1137

18 Erdogmus, S. *et al.* Helix 8 is the essential structural motif of mechanosensitive GPCRs. *Nat Commun* **10**, 5784 (2019). https://doi.org:10.1038/s41467-019-13722-0

19 Hoffmann, E. K., Lambert, I. H. & Pedersen, S. F. Physiology of cell volume regulation in vertebrates. *Physiol Rev* **89**, 193-277 (2009). https://doi.org:10.1152/physrev.00037.2007
20 Roffay, C. *et al.* Passive coupling of membrane tension and cell volume during active response of cells to osmosis. *Proc Natl Acad Sci U S A* **118** (2021). https://doi.org:10.1073/pnas.2103228118
21 Liu, X. *et al.* Structural Insights into the Process of GPCR-G Protein Complex Formation. *Cell* **177**, 1243-1251 e1212 (2019). https://doi.org:10.1016/j.cell.2019.04.021
22 Scarselli, M., Annibale, P. & Radenovic, A. Cell type-specific beta2-adrenergic receptor clusters identified using photoactivated localization microscopy are not lipid raft related, but depend on actin cytoskeleton integrity. *J Biol Chem* **287**, 16768-16780 (2012). https://doi.org:10.1074/jbc.M111.329912
23 van Unen, J. *et al.* A New Generation of FRET Sensors for Robust Measurement of Galphai1, Galphai2 and Galphai3 Activation Kinetics in Single Cells. *PLoS One* **11**, e0146789 (2016). https://doi.org:10.1371/journal.pone.0146789
24 Klarenbeek, J., Goedhart, J., van Batenburg, A., Groenewald, D. & Jalink, K. Fourth-generation epac-based FRET sensors for cAMP feature exceptional brightness, photostability and dynamic range: characterization of dedicated sensors for FLIM, for ratiometry and with high affinity. *PLoS One* **10**, e0122513 (2015). https://doi.org:10.1371/journal.pone.0122513
25 Vandenberg, J. I., Rees, S. A., Wright, A. R. & Powell, T. Cell swelling and ion transport pathways in cardiac myocytes. *Cardiovasc Res* **32**, 85-97 (1996).
26 Drake, M. T., Shenoy, S. K. & Lefkowitz, R. J. Trafficking of G protein-coupled receptors. *Circ Res* **99**, 570-582 (2006). https://doi.org:10.1161/01.RES.0000242563.47507.ce
27 Beavo, J. A. *et al.* Effects of xanthine derivatives on lipolysis and on adenosine 3',5'-monophosphate phosphodiesterase activity. *Mol Pharmacol* **6**, 597-603 (1970).
28 Tesmer, J. J., Sunahara, R. K., Gilman, A. G. & Sprang, S. R. Crystal structure of the catalytic domains of adenylyl cyclase in a complex with Gsalpha.GTPgammaS. *Science* **278**, 1907-1916 (1997). https://doi.org:10.1126/science.278.5345.1907
29 Sunahara, R. K., Dessauer, C. W., Whisnant, R. E., Kleuss, C. & Gilman, A. G. Interaction of Gsalpha with the cytosolic domains of mammalian adenylyl cyclase. *J Biol Chem* **272**, 22265-22271 (1997). https://doi.org:10.1074/jbc.272.35.22265
30 Vortherms, T. A., Nguyen, C. H., Bastepe, M., Juppner, H. & Watts, V. J. D2 dopamine receptor-induced sensitization of adenylyl cyclase type 1 is G alpha(s) independent. *Neuropharmacology* **50**, 576-584 (2006). https://doi.org:10.1016/j.neuropharm.2005.11.004
31 Stallaert, W. *et al.* Purinergic Receptor Transactivation by the beta(2)-Adrenergic Receptor Increases Intracellular Ca(2+) in Nonexcitable Cells. *Mol Pharmacol* **91**, 533-544 (2017). https://doi.org:10.1124/mol.116.106419
32 Westfield, G. H. *et al.* Structural flexibility of the G alpha s alpha-helical domain in the beta2-adrenoceptor Gs complex. *Proc Natl Acad Sci U S A* **108**, 16086-16091 (2011). https://doi.org:10.1073/pnas.1113645108
33 Axelrod, D. Total internal reflection fluorescence microscopy. *Methods Cell Biol* **30**, 245-270 (1989). https://doi.org:10.1016/s0091-679x(08)60982-6
34 Nygaard, R. *et al.* The dynamic process of beta(2)-adrenergic receptor activation. *Cell* **152**, 532-542 (2013). https://doi.org:10.1016/j.cell.2013.01.008
35 Lakowicz, J. R. *Principles of fluorescence spectroscopy*. 2nd edn, (Kluwer Academic/Plenum, 1999).
36 Rasmussen, S. G. *et al.* Structure of a nanobody-stabilized active state of the beta(2) adrenoceptor. *Nature* **469**, 175-180 (2011). https://doi.org:10.1038/nature09648
37 Koster, D. V. & Mayor, S. Cortical actin and the plasma membrane: inextricably intertwined. *Curr Opin Cell Biol* **38**, 81-89 (2016). https://doi.org:10.1016/j.ceb.2016.02.021
38 Haussinger, D. The role of cellular hydration in the regulation of cell function. *Biochem J* **313 (Pt 3)**, 697-710 (1996). https://doi.org:10.1042/bj3130697

39 Tang, W., Strachan, R. T., Lefkowitz, R. J. & Rockman, H. A. Allosteric modulation of beta-arrestin-biased angiotensin II type 1 receptor signaling by membrane stretch. *J Biol Chem* **289**, 28271-28283 (2014). https://doi.org:10.1074/jbc.M114.585067
40 Groulx, N., Boudreault, F., Orlov, S. N. & Grygorczyk, R. Membrane reserves and hypotonic cell swelling. *J Membr Biol* **214**, 43-56 (2006). https://doi.org:10.1007/s00232-006-0080-8
41 Lang, F. *et al.* Functional significance of cell volume regulatory mechanisms. *Physiol Rev* **78**, 247-306 (1998). https://doi.org:10.1152/physrev.1998.78.1.247
42 Sinha, B. *et al.* Cells respond to mechanical stress by rapid disassembly of caveolae. *Cell* **144**, 402-413 (2011). https://doi.org:10.1016/j.cell.2010.12.031
43 Steinberg, S. F. beta(2)-Adrenergic receptor signaling complexes in cardiomyocyte caveolae/lipid rafts. *J Mol Cell Cardiol* **37**, 407-415 (2004). https://doi.org:10.1016/j.yjmcc.2004.04.018
44 Allen, J. A. *et al.* Caveolin-1 and lipid microdomains regulate Gs trafficking and attenuate Gs/adenylyl cyclase signaling. *Mol Pharmacol* **76**, 1082-1093 (2009). https://doi.org:10.1124/mol.109.060160
45 Guo, Y., Yang, L., Haught, K. & Scarlata, S. Osmotic Stress Reduces Ca2+ Signals through Deformation of Caveolae. *J Biol Chem* **290**, 16698-16707 (2015). https://doi.org:10.1074/jbc.M115.655126
46 DiPilato, L. M. & Zhang, J. The role of membrane microdomains in shaping beta2-adrenergic receptor-mediated cAMP dynamics. *Mol Biosyst* **5**, 832-837 (2009). https://doi.org:10.1039/b823243a
47 Irannejad, R. *et al.* Conformational biosensors reveal GPCR signalling from endosomes. *Nature* **495**, 534-538 (2013). https://doi.org:10.1038/nature12000
48 Fried, S. D. E. *et al.* Hydration-mediated G-protein-coupled receptor activation. *Proc Natl Acad Sci U S A* **119**, e2117349119 (2022). https://doi.org:10.1073/pnas.2117349119
49 Tolkovsky, A. M. & Levitzki, A. Mode of coupling between the beta-adrenergic receptor and adenylate cyclase in turkey erythrocytes. *Biochemistry* **17**, 3795 (1978). https://doi.org:10.1021/bi00611a020
50 Pena-Rasgado, C., Kimler, V. A., McGruder, K. D., Tie, J. & Rasgado-Flores, H. Opposite roles of cAMP and cGMP on volume loss in muscle cells. *Am J Physiol* **267**, C1319-1328 (1994). https://doi.org:10.1152/ajpcell.1994.267.5.C1319
51 Meng, X. J. & Weinman, S. A. cAMP- and swelling-activated chloride conductance in rat hepatocytes. *Am J Physiol* **271**, C112-120 (1996). https://doi.org:10.1152/ajpcell.1996.271.1.C112
52 Carpenter, E. & Peers, C. Swelling- and cAMP-activated Cl- currents in isolated rat carotid body type I cells. *J Physiol* **503 (Pt 3)**, 497-511 (1997). https://doi.org:10.1111/j.1469-7793.1997.497bg.x
53 Golstein, P. E. *et al.* Hypotonic cell swelling stimulates permeability to cAMP in a rat colonic cell line. *Pflugers Arch* **447**, 845-854 (2004). https://doi.org:10.1007/s00424-003-1216-7
54 Hynes, T. R., Mervine, S. M., Yost, E. A., Sabo, J. L. & Berlot, C. H. Live cell imaging of Gs and the beta2-adrenergic receptor demonstrates that both alphas and beta1gamma7 internalize upon stimulation and exhibit similar trafficking patterns that differ from that of the beta2-adrenergic receptor. *J Biol Chem* **279**, 44101-44112 (2004). https://doi.org:10.1074/jbc.M405151200
55 Bathe-Peters, M., Gmach, P., Annibale, P. & Lohse, M. J. Linescan microscopy data to extract diffusion coefficient of a fluorescent species using a commercial confocal microscope. *Data Brief* **29**, 105063 (2020). https://doi.org:10.1016/j.dib.2019.105063
56 Jaqaman, K. *et al.* Robust single-particle tracking in live-cell time-lapse sequences. *Nat Methods* **5**, 695-702 (2008). https://doi.org:10.1038/nmeth.1237